Supplementary Information

Multiscale structural control of MFI zeolite using poly-quaternary ammonium cation

Yingjie Zhou,‡[a] Quanzheng Deng,‡[b] Donghao Deng,‡[c] Wei Liu,[c] Miao Zhai,§[a] Zhendong Wang,[c] Lu Han*[b] and Kake Zhu*[a]*

[a] State Key Laboratory of Chemical Engineering, School of Chemical Engineering, East China University of Science and Technology, Shanghai, 200237, P. R. China.

[b] School of Chemical Science and Engineering, Tongji University, Shanghai, 200092, P. R. China.

[c] State Key Laboratory of Green Chemical Engineering and Industrial Catalysis; SINOPEC Shanghai Research Institute of Petrochemical Technology Co., Ltd., Shanghai, 201208, P. R. China.

§Department of Food and Biochemical Engineering, Yantai Vocational College, Yantai, 264670, P. R. China.

‡These authors contributed equally to the work.

[*] Email: wangzd.sshy@sinopec.com. luhan@tongji.edu.cn. kakezhu@ecust.edu.cn.

Table of Contents

1. Experimental

1.1 Chemicals and Reagents

1,5-dibromopentane ($C_5H_{10}Br_2$, 98.0%), 1,6-dibromohexane ($C_6H_{12}Br_2$, 98.0%), 1,7-dibromoheptane ($C_7H_{14}Br_2$, 98.0%), dipropylamine ($C_6H_{15}N$, 99.0%), tetraethyl orthosilicate (TEOS, 28.0 wt.% SiO_2), sodium aluminate ($NaAlO_2$), aluminum hydroxides ($Al(OH)_3$, 99.9%) tetrapropylammonium hydroxide solution (TPAOH, 25.0 wt.% in water) were taken from Shanghai Aladdin Biochemical Technology Co., Ltd. Ethylbutylamine ($C_6H_{15}N$, 99.0%), sodium hydroxide (NaOH, 98.0 wt.%) were supplied by Shanghai Titan Reagents Co. Ltd. Glutaryl chloride ($C_5H_6Cl_2O_2$, 97.0%), adipoyl chloride ($C_6H_8Cl_2O_2$, 98.0%), magnesium sulfate anhydrous ($MgSO_4$, 99.0% metals basis), sodium bicarbonate ($NaHCO_3$, 99.8%) were purchased from Shanghai Macklin Biochemical Technology Co., Ltd. N,N- diisopropylethylamine ($C_8H_{19}N$, 99.0%, ultradry, with molecular sieves, water ≤ 50 ppm (by K. F.)), silver oxide (Ag_2O, 99.0%) were taken from Shanghai Meryer Biochemical Technology Co., Ltd. Lithium aluminum hydride ($LiAlH_4$, 97.0%), tetrahydrofuran (THF, 99.5%, ultradry, with molecular sieves, stabilized with 250 ppm BHT, J&K Seal), acetonitrile (MeCN, 99.9%, ultradry, water ≤ 30 ppm J&K Seal), methyl alcohol (MeOH, 99.9%, ultradry, water ≤ 30 ppm J&K Seal), ethyl acetate ($C_4H_8O_2$, 99.0%) were taken from Shanghai J&K Scientific Co. Ltd.

1.2 Synthesis of Monomer Precursors

Other monomer precursors, including N,N,N',N'-tetrapropyl-1,5-pentanediamine, N,N'-dibutyl-N,N'-diethyl-1,6-hexanediamine and N,N'-dibutyl-N,N'-diethyl-1,5-pentanediamine, were synthesized by reacting the corresponding acyl chloride with dipropylamine and ethylbutylamine, respectively, to afford N,N,N',N'-tetrapropyl-1,5-pentanediamide, N,N'-dibutyl-N,N'-diethyl-1,6-hexanediamide and N,N'-dibutyl-N,N'-diethyl-1,5-

pentanediamine. The resultant products were reduced with $LiAlH_4$ to the corresponding amides. In a typical synthesis, dipropylamine (0.40 mol) was dissolved into 500.00 mL dehydrated THF in a flask at 273 K and stirred for 1 h, to which glutaryl chloride (0.10 mol) was charged and the mixture was vigorously stirred at 293 K for 48 h. The solid was filtered off and the supernatant solution was mixed with 5 wt.% $NaHCO_3$ aqueous solution, to obtain a biphasic liquid mixture. The upper organic phase was separated, dried with $MgSO_4$ for 24 h, and the solid was filtered off. Subsequently, the THF in the solution was evaporated, yielding a yellowish liquid N,N,N',N'-tetrapropyl-1,5-pentanediamide. N,N,N',N'-tetrapropyl-1,5-pentanediamine was produced after the reduction of N,N,N',N'-tetrapropyl-1,5-pentanediamide (0.10 mol) by $LiAlH_4$ (0.40 mol) dissolved in 600.00 mL THF at 333 K for 48 h under stirring. The monomer precursor was produced after quenching by sequential addition of 16.00 mL MeOH, 16.00 mL H_2O and 16.00 g $MgSO_4$ at 273 K, filtration to remove solid residues and rotary evaporation to dryness.

1.3 Synthesis of Poly-quaternary Ammonium Cations

Poly-quaternary ammonium cations $–N^+(CH_2CH_2CH_3)_2–(CH_2)_5–N^+(CH_2CH_2\ CH_3)_2–(CH_2)_7–$, (abbreviated as -$NPr_2$-$C_5$- NPr_2-C_7-), $–N^+(CH_2CH_3)(CH_2CH_2CH_2CH_3)–(CH_2)_6–$ (abbreviated as -NEtBu-C_6-), $–N^+(CH_2CH_3)(CH_2CH_2CH_2CH_3)–(CH_2)_5–N^+(CH_2CH_3)(CH_2CH_2\ CH_2CH_3)–(CH_2)_7–$ (abbreviated as -NEtBu-C_5-NEtBu-C_7-) were synthesized by polymerizing of the corresponding diamines (detailed synthesis procedures were illustrated in Supplementary Experimental Procedures, Fig. S26) derived above with dibromoalkane. The synthesis processes were consistent with -NPr_2-C_6-. The synthesis of -NEtBu-C_5-NEtBu-C_7- was extended to 96 h.

1.4 Synthesis of Conventional ZSM-5-C Zeolite

TPAOH (25 wt.% in water), deionized H_2O, NaOH and $NaAlO_2$ were mixed until a clear suspension was obtained. TEOS was added dropwise into the above solution. The molar

composition of the mixture was set to 1 SiO_2: 0.01 Al_2O_3: 0.08 NaOH: 0.20 TPAOH: 25 H_2O: 4 EtOH. Crystallization was conducted in a convection oven at 443 K for 48 h under static conditions. The obtained product was centrifuged, washed with deionized water, dried at 353 K for 8 h in a convection oven, and calcined in air at 823 K for 6 h with a heating rate of 2 K min^{-1} in a muffle oven. To prepare H-type zeolite, the 1.00 g calcined product was ion-exchanged in 100.00 mL 1.00 M NH_4Cl solution at 353 K for 12 h, followed by washing with deionized water and calcination at 823 K for 5 h. The obtained sample was denoted as ZSM-5-C-(50).

1.5 Characterizations

Liquid-state ^1H and ^{13}C nuclear magnetic resonance (NMR) spectra were recorded by a JEOL spectrometer at 500 MHz. The molecular weight of the hydroxide form poly-quaternary ammonium cations was measured by Gel Permeation Chromatography (GPC) on the WATERS 2414 differential refractive index detector equipped with WATERS ULtrahydrogel × 3 gel column. The mobile phase is 0.10 M aqueous solution of sodium nitrate. Polyethylene glycol was used as standard sample. The temperature of column and detectors were 313 K. Powder X-ray diffractions (XRD) patterns of samples were systematically analyzed on Rigaku D/Max 2550 VB/PC diffractometer, which was operated at 100 mA and 40 kV using Cu Kα (λ = 1.5418 Å) as X-ray source. Relative crystallinity was calculated by the ratio of the integrated areas of the peaks at 2θ range from 7.4 to 9.2, 22.0 to 25.2. Field emission scanning electron micrographs were captured in Field-Emission Scanning Electron Microscopy (FE-SEM) NOVA Nano SEM 450 (FEI). The elemental compositions of samples were determined by Inductively Coupled Plasma Atomic Emission Spectrometry (ICP-AES) conducted on an IRIS 1000 (Agilent Technologies, USA) and vario EL cube Elemental Analyzer (Elementar, Germany). Argon (Ar) adsorption-desorption isotherm measurements were performed on an ASAP 2460 (Micromeritics, USA) at 87 K after the

samples were degassed at 573 K for 12 h under vacuum. The specific surface area (S_{BET}) was calculated using Brunauer-Emmett-Teller (BET) equation at relative pressure P/P_0 = 0.05–0.30 using the adsorption branch data. The micropore area (S_{micro}), external surface area (S_{ext}), and micropore volume (V_{micro}) were obtained by *t*-plot method. The total pore volume (V_{total}) was estimated by single point method at a relative pressure of P/P_0 = 0.99. The pore-size distributions were obtained by Non-local Density Functional Theory (NLDFT) method from the adsorption branch using the Ar@87 zeolites, Me-form, cylindrical pore model. Thermogravimetric analysis (TGA) of samples was measured on a vacuum-sealed synchronous TGA-DSC thermal analyzer STA 449 F5 Jupiter (Netzsch). The samples were heated from room temperature to 1073 K with a heating rate of 10 K min^{-1} under air atmosphere. Transmission Electron Microscope (TEM), high-resolution TEM (HRTEM) and electron tomography were performed using the JEOL JEM-F200 FEG TEM operating at an accelerating voltage of 200 kV, together with an RIO-16 camera which has a built-in drift correction function, and a high tilt holder (EM-21010/21340). A tilt series of TEM images were then collected over an angular range from −60 to +60° at an interval of 3.0°. Tomviz software package was then used for tilt series data processing. The GENFIRE algorithm was utilized for reconstruction, and the final visualization was also performed using Tomviz. ^{27}Al magic angle spinning (MAS), ^{13}C cross-polarization (CP) MAS, ^{1}H MAS, ^{29}Si MAS, ^{1}H-^{13}C heteronuclear correlation (HETCOR), ^{1}H-^{29}Si HETCOR were performed on a Bruker Ascend 600 spectrometer (14.1 T) with resonance frequencies of 600.13 MHz, 156.38 MHz, 119.2 MHz and 150.92 MHz for ^{1}H, ^{27}Al, ^{29}Si and ^{13}C, respectively. ^{13}C CP MAS NMR spectra were acquired on a 3.2 mm MAS NMR probe with a spinning rate of 18 kHz, contact time of 2 ms at a recycle delay of 2 s. ^{1}H-^{13}C HETCOR experiments were conducted with a CP contact time of 2 ms at a spinning rate of 18 kHz and a recycle delay of 2 s, scan number of 480 for each t1 increment.

All these samples were dehydrated at 353 K under a pressure of $<10^{-3}$ Pa over 10 h. ^{29}Si MAS NMR spectrum was recorded on a 7 mm probe with a spinning rate of 4 kHz, a π/4 pulse length of 3 μs, a recycle delay of 45 s. ^{27}Al MAS NMR experiments were performed using a 3.2 mm MAS NMR probe with a spinning rate of 18 kHz, a π/12 pulse length of 0.36 μs and a repetition time of 0.5 s. The ^{27}Al chemical shifts were referenced to a 1 M aqueous solution of $Al(NO_3)_3$. ^{1}H-^{27}Al HETCOR experiments were conducted with a CP contact time of 5 ms at a spinning rate of 18 kHz and a recycle delay of 2 s, scan number of 1600 for each t1 increment. ^{1}H-^{29}Si HETCOR experiments were conducted with a CP contact time of 1.5 ms at a spinning rate of 18 kHz and a recycle delay of 2 s, scan number of 240 for each t1 increment. ^{29}Si chemical shift were referenced to tetramethylsilane (TMS). The Fourier-transform infrared spectra (FT-IR) over ZSM-5 samples were recorded using a Nicolet-iS50 spectrometer. Prior to the measurements, the samples were pressed into self-supporting wafers (diameter: 1.3 cm, 25.00 mg) and preheated in an IR cell attached to a vacuum line at 773 K (2 K min^{-1}) for 3 h down to 10^{-4} MPa. Pyridine Infrared Spectroscopy (Py-IR) was used to detect the types and quantities of acid sites of samples using a Nicolet-iS50 spectrometer. All samples were degassed at 773 K for 1 h, and then collected the background baselines of the samples at the corresponding test temperature (573 K, 423 K) in turn. Pyridine was introduced on the sample at ambient temperature for 30 min. Spectrogram was recorded after desorbing pyridine at 423 K, 573 K. The quantification of Brønsted (B) and Lewis (L) acid site densities was calculated from the relevant extinction coefficients, molar extinction coefficients 1.67 cm $μmol^{-1}$ and 2.22 cm $μmol^{-1}$, for vibration at 1545 cm^{-1} and 1455 cm^{-1}, respectively.[1] NH_3 temperature programmed desorption (NH_3-TPD) was used to characterize acidic by an Auto Chem II chemisorption instrument (Micromeritics Co., USA).

1.6 Diffusivity Measurements

The diffusivity of 2-methylhexane (2-MC_6) inside ZSM-5 crystals was measured using gravimetry on an Intelligent Gravimetric Analyzer, model IGA-100 (Hiden Analytical Ltd., UK). The characterization was carried with a reported procedure described in our previous article.[2]

At the initial stage of the adsorption process on ZSM-5 crystals, the solution of this equation could be well approximated as follows:

$$\frac{q(t)}{q(\infty)} = \frac{6}{\sqrt{\pi}}\sqrt{\frac{D_{eff}}{L^2}}\sqrt{t} \qquad (1)$$

whereby $\frac{q(t)}{q(\infty)}$ was the normalized 2-MC_6 adsorption, D_{eff} was the diffusion coefficient and L was the characteristic diffusion length. Fitting of uptake curves generated $\frac{D_{eff}}{L^2}$, known as diffusion characteristic constant.

1.7 Catalytic Assessments

***n*-Heptane catalytic cracking reaction.** The *n*-heptane catalytic cracking reaction was conducted in a corundum tubular fixed-bed reactor with an inner diameter of 10 mm under atmosphere pressure at 873 K. 0.42 g ZSM-5 catalysts was pressurized, ground and sieved into pellets of 20–40 mesh, and was diluted with 5.00 g quartz sand before mounting into the reactor. The reactant *n*-heptane was injected by constant flow pump with a flow rate of 0.02 mL min^{-1}, mass space velocity (WHSV) of *n*-heptane was kept to 2.00 $g_{n\text{-heptane}}\ h^{-1}\ g_{cat}^{-1}$ and N_2 flow rate of 30 mL min^{-1}. The composition of the product was analyzed by gas chromatograph (GC) GC-2014 from Shimadzu, Japan, and the product was determined by flame ionization detector (FID). The chromatographic column was a capillary column (OA-101, 50 m × 0.53 mm × 0.50 μm), the

temperature of the detector was 473 K, and the column temperature was first maintained at 323 K for 6 min, and then increased to 423 K at 8 K min^{-1} for 20 min. with Ar carrier gas. The conversion and selectivities were calculated as follows, while the integral product selectivities were deduced following Bhan et al.[3] after subtracting contributions from non-catalytic thermal cracking (derived from blank test).

$$\text{Conversion} = (1 - \frac{\text{C atoms of } n\text{-heptane output}}{\text{C atoms of } n\text{-heptane input}}) \times 100\% \quad (2)$$

$$\text{Integral product selectivity} = (\frac{\text{C atoms of } C_{n,\,t_1} \text{ product}}{\sum \text{C atoms of } C_{n,\,t_1} \text{ product}}) \times 100\% = (\frac{\frac{\int_0^{t_1} (N_{C_{n,\,t}} - N_{C_{n,\,t_1}}) n \, dt}{M_{w,\,n}}}{\sum \text{C atoms of } C_{n,\,t_1} \text{ product}}) \times 100\% \quad (3)$$

$C_{n,\,t}$: products C_n with n carbon at time on stream of t, t_1 is the deactivation time of the catalyst, $N_{C_{n,\,t}}$: the number of C atoms of C_n at time on stream, $M_{w,\,n}$: molar molecular weight of products C_n.

The turnover number (TON) was calculated from the following equation proposed by Bhan et al.,[3]

$$\text{TON} = \frac{F_{n\text{-heptane}} \times \int_0^t (x_{n\text{-heptane},\,t}\, dt)}{n_{Al}} \quad (4)$$

$F_{n\text{-heptane}}$: the flow rate of n-heptane, t: the reaction time when n-heptane conversion rate is reduced to 23%, $x_{n\text{-heptane},\,t}$: the transient conversion rate of n-heptane at time on stream of t, n_{Al}: the total number of accessible Brønsted and Lewis acid sites calculated from Py-IR.

$$R_{coke}\ (\text{mg h}^{-1}) = coke \text{ amount (mg)} / \text{reaction time (h)} \quad (5)$$

$$P_{coke}\ (\text{mg g}_{n\text{-heptane}}^{-1}) = coke \text{ amount (g)} / n\text{-heptane feedstock (g)} \quad (6)$$

2. Supplementary Tables

Table S1. Gel permeation chromatography (GPC) analysis of poly quaternary cations.

Samples	Distribution	Mn	Mw	Mp	Polydispersity[a]	n[b]
-NPr_2-C_6-	1	1021	1055	1028	1.03	6
	2	1881	31328	29633	1.66	159
-NPr_2-C_5-NPr_2-C_7-	1	8535	9026	8942	1.08	24
	2	21743	2337	2291	1.08	6
	3	933	970	962	1.04	3
-NEtBu-C_6-	1	2177	2416	2833	1.11	15
-NEtBu-C_5-NEtBu-C_7-	1	16723	21447	18094	1.28	49
The supernatant liquor at the end of crystallization using -NPr_2-C_6-	1	1279	1565	1156	1.2	6

[a]Polydispersity = Molecular weight (Mw)/ number-average molecular weight (Mn).

[b]n = Molecular weight (Mp)/ Molar molecular weight of corresponding repeating segment.

Table S2. Elemental analysis (EA) and inductively coupled plasma atomic emission spectrometry (ICP-AES) results of as-synthesized zeolites.

Samples	EA (wt.%)[a]			C/N	ICP-AES (wt.%)[b]			Si/Al[b]	N/Si[a]	Theoretical N/Si[c]	Stoichiometry
	C	N	H		Na	Si	Al				
ZSM-5-NPr$_2$-C$_6$-(50)	13.63	1.32	2.93	12.04	0.06	30.60	0.68	43	0.086	0.021	$\|Na_{0.20}$-$SEG_{1.97}$-$(H_2O)_{19}\|$ **[**$Si_{93.83}Al_{2.17}O_{192}$**]-MFI**
ZSM-5-NPr$_2$-C$_6$-(100)	13.75	1.27	2.73	12.63	0.03	32.40	0.36	86	0.079	0.010	$\|Na_{0.11}$-$SEG_{0.99}$-$(H_2O)_{14}\|$ **[**$Si_{94.90}Al_{1.10}O_{192}$**]-MFI**
ZSM-5-NPr$_2$-C$_6$-(∞)	12.96	1.22	2.56	12.39	0.01	33.00	-		0.074	0.074	-
ZSM-5-NPr$_2$-C$_6$-(50)-Na free	-	-	-	-	-	38.30	0.82		-	-	-
ZSM-5-C-(50)	8.32	0.80	1.92	12.13	0.58	33.20	0.66	48	-	-	$\|Na_{1.93}$-$TPA_{0.02}$-$(H_2O)_{16}\|$ **[**$Si_{94.05}Al_{1.95}O_{192}$**]-MFI**

[a]Determined by elemental analysis. [b]Calculated by inductively coupled plasma atomic emission spectrometry. [c]Calculated by stoichiometry of products.

Table S3. Selectivity, TON, CMR, *O/P*, R_{coke} and P_{coke} in the *n*-heptane catalytic cracking over samples.

		Catalysts	
		ZSM-5-C-(50)	ZSM-5-NPr_2-C_6-(50)
Selectivity (%)[a]	C_1	1.7	11.0
	C_2	2.8	11.1
	$C_2^=$	8.7	20.6
	C_3	19.0	6.1
	$C_3^=$	30.9	31.6
	i-C_4	2.6	0.4
	n-C_4	11.5	3.8
	$C_4^=$	18.7	9.2
	C_5	2.5	2.4
	BTX	1.6	3.7
	$C_2^= + C_3^=$	39.6	52.2
TON[b]		2.96×10^4	1.50×10^5
CMR[c]		5.06	95.50
O/P[d]		1.81	3.03
R_{coke} (mg min^{-1})		0.0104	0.0056
P_{coke} (mg $g_{n\text{-hepane}}^{-1}$)		0.0127	0.0068

[a] $\text{Selectivity} = \frac{\text{C atoms of } C_{n,\,t_1} \text{ product}}{\sum \text{C atoms of } C_{n,\,t_1} \text{ product}}$ [b] $\text{TON} = \frac{F_{n\text{-heptane}} \times \int_0^t (x_{n\text{-heptane},\,t}\,\mathrm{d}t)}{n_{\mathrm{Al}}}$ [c]Defined as the ratio $(C_1 + C_2 + C_2^=)/i\text{-}C_4$, where C_1, C_2, $C_2^=$ and *i*-C_4 denote the molar selectivities to methane, ethane, ethene and *i*-butane, respectively. [d]$C_n/C_n^=$ (n = 2–3).

Table S4. Crystallization conditions using polycationic OSDAs.

Molar composition of precursor gel	Synthesis Time
1 SiO_2: 0.01 Al_2O_3: 0.30 -NPr_2-C_6-: 0.15 NaOH: (10-150) H_2O: 4 EtOH	144 h
1 SiO_2: 0.01 Al_2O_3: 0.20 -NPr_2-C_6-: 0.15 NaOH: 150 H_2O: 4 EtOH	120 h
1 SiO_2: 0.01 Al_2O_3: 0.20 -NPr_2-C_6-: 0.10 NaOH: 150 H_2O: 4 EtOH	168 h
1 SiO_2: 0.01 Al_2O_3: 0.20 -NPr_2-C_6-: (0 /0.02) NaOH: 150 H_2O: 4 EtOH	288 h
1 SiO_2: 0.01 Al_2O_3: 0.30 -NPr_2-C_6-: (0.10/0.15) NaOH: 150 H_2O: 4 EtOH	120 h
1 SiO_2: 0.01 Al_2O_3: 0.30 -NPr_2-C_6-: (0/0.02) NaOH: 150 H_2O: 4 EtOH	192 h
1 SiO_2: 0.01 Al_2O_3: 0.42 -NPr_2-C_6-: (0.10/0.15) NaOH: 150 H_2O: 4 EtOH	120 h
1 SiO_2: 0.01 Al_2O_3: 0.42 -NPr_2-C_6-: (0/0.02) NaOH: 150 H_2O: 4 EtOH	216 h
1 SiO_2: *x* Al_2O_3: 0.20 -NPr_2-C_6-: 0.15 NaOH: 150 H_2O: 4 EtOH (Si/Al = 10, 25)	288 h
1 SiO_2: *x* Al_2O_3: 0.20 -NPr_2-C_6-: 0.15 NaOH: 150 H_2O: 4 EtOH (Si/Al = 100, 150 and ∞)	192 h
1 SiO_2: 0.01 Al_2O_3: 0.20 -NEtBu-C_6-: 0.15 NaOH: 150 H_2O: 4 EtOH	312 h
1 SiO_2: 0.01 Al_2O_3: 0.10 OSDAs: 0.15 NaOH: 150 H_2O: 4 EtOH	120 h

OSDAs = -NPr_2-C_5-NPr_2-C_7-, -NEtBu-C_5-NEtBu-C_7-
Hydrothermal temperature: 438 K

3. Supplementary Figures

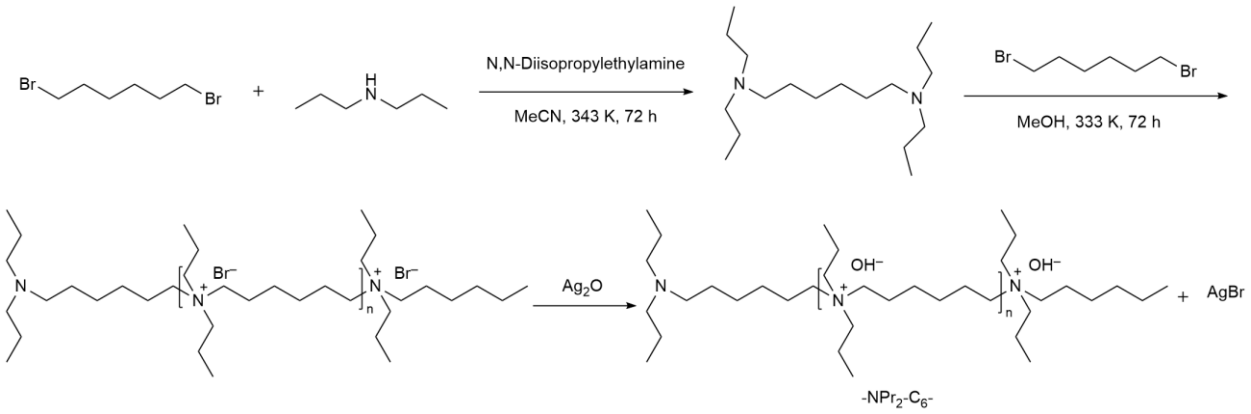

Fig. S1 Synthesis of monomer precursor N,N,N',N'-tetrapropyl-1,6-hexanediamine, poly-quaternary ammonium bromide and poly-quaternary ammonium cation (-NPr_2-C_6-).

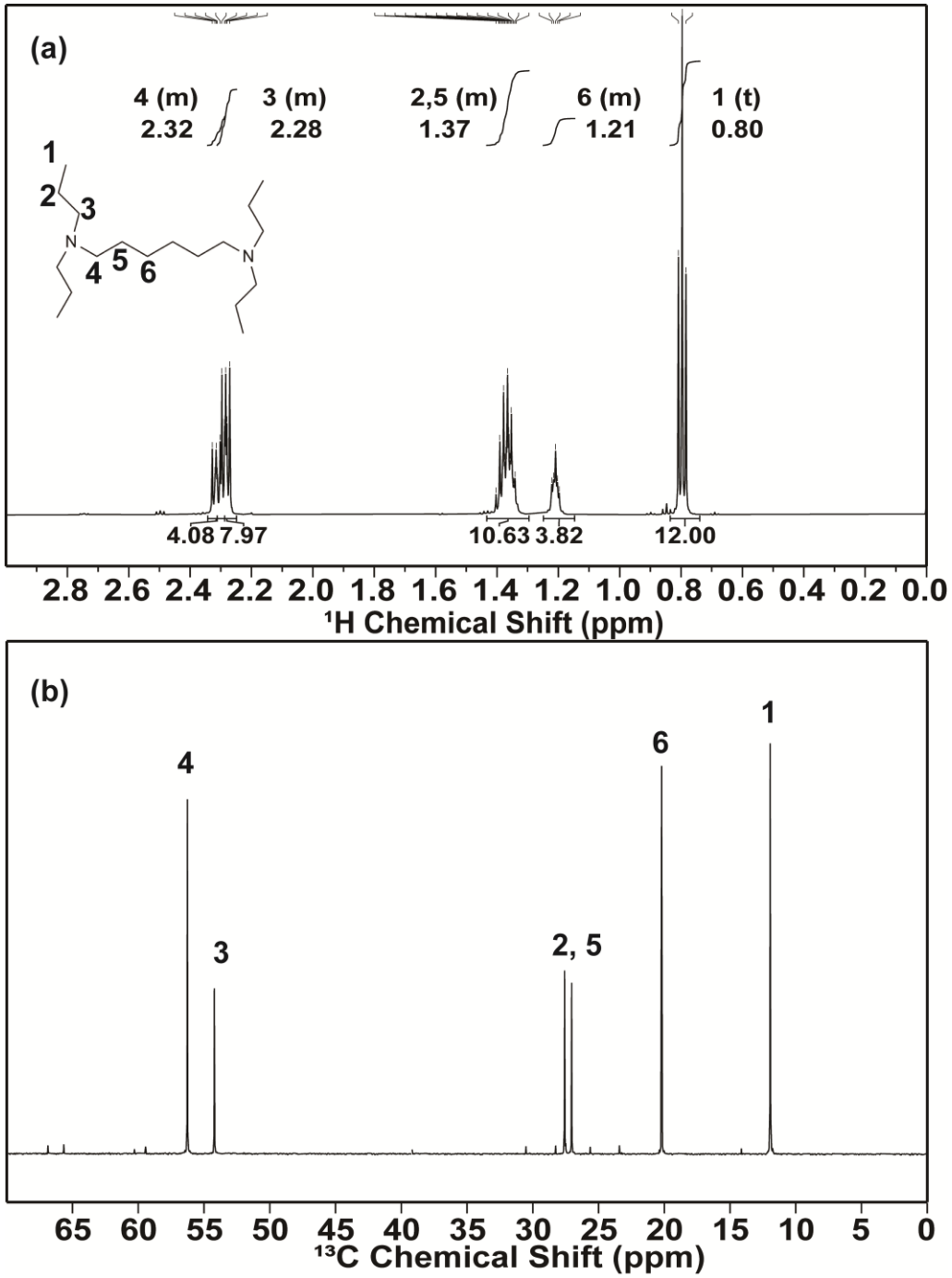

Fig. S2 ^{1}H (a) and ^{13}C (b) nuclear magnetic resonance (NMR) spectra of N,N,N',N'-tetrapropyl-1,6-hexanediamine dissolved in $CDCl_3$.

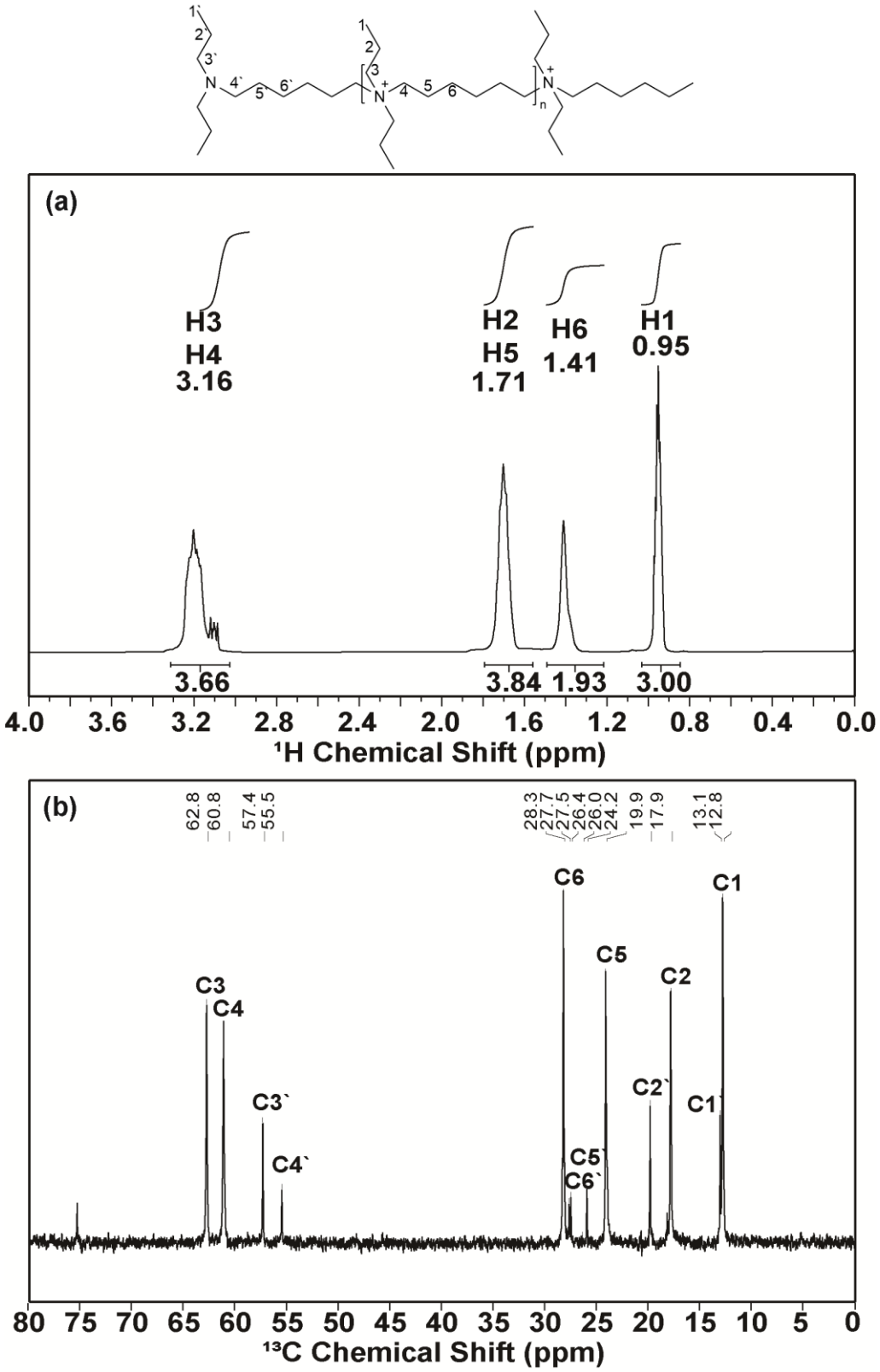

Fig. S3 ^{1}H (a) and ^{13}C (b) NMR spectra of poly-quaternary ammonium bromide dissolved in D_2O.

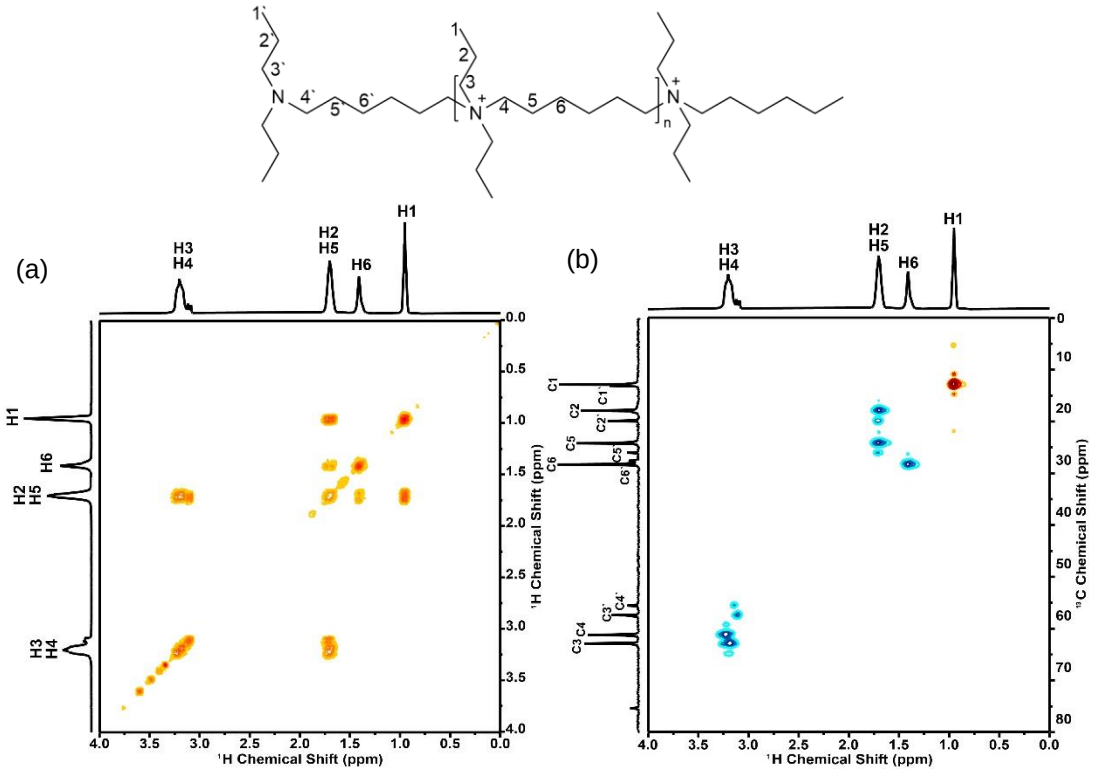

Fig. S4 ^{1}H-^{1}H correlation spectroscopy (COSY) NMR spectra (a), ^{13}C-^{1}H heteronuclear single-quantum correlation spectroscopy (HSQC) NMR spectra (b) of -NPr$_2$-C$_6$- dissolved in D$_2$O. The ^{1}H-^{1}H COSY NMR spectrum generally reflects the coupling relationship of hydrogens on neighboring carbons. The signals outside the diagonal are called cross peaks, which indicate the coupling between hydrogen atoms. H1-3-4-6 is coupled to H2 and H5. ^{13}C-^{1}H HSQC 2D NMR spectra describe the relationship of hydrogen and carbon nuclei separated by one covalent bond. 2D NMR spectra further verified the structure of -NPr$_2$-C$_6$-.

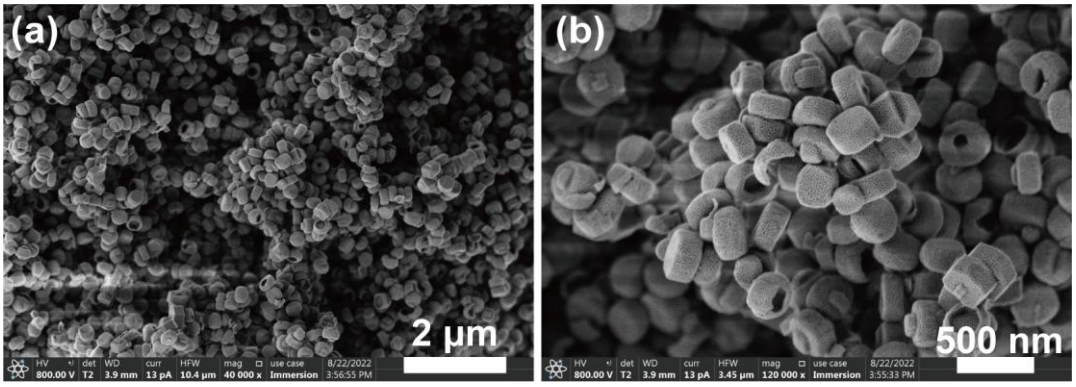

Fig. S5 FE-SEM micrographs for as-synthesized ZSM-5-C-(50).

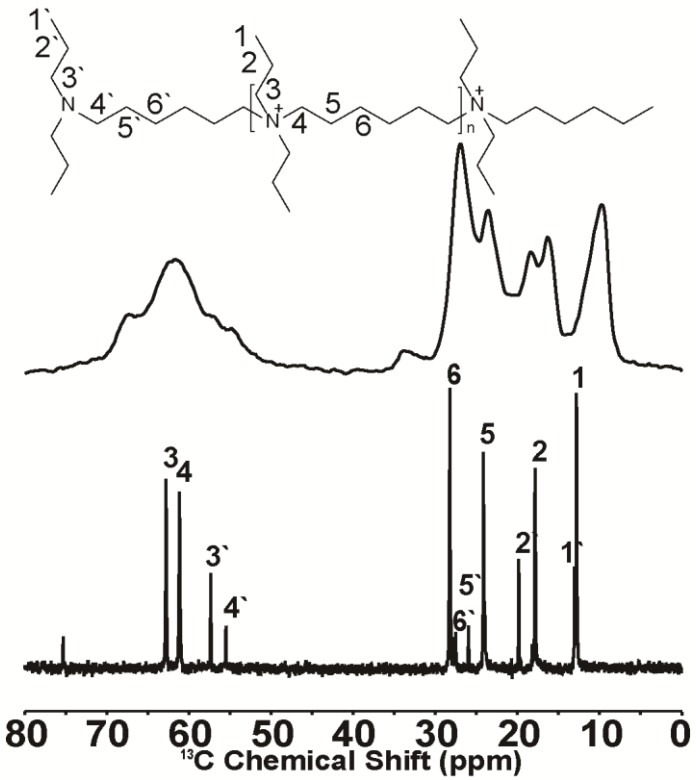

Fig. S6 ^{13}C cross-polarization magic angle spinning (CP MAS) NMR spectra (top) of as-synthesized ZSM-5-NPr_2-C_6-(50) and ^{13}C NMR spectra (bottom) of -NPr_2-C_6- dissolved in D_2O.

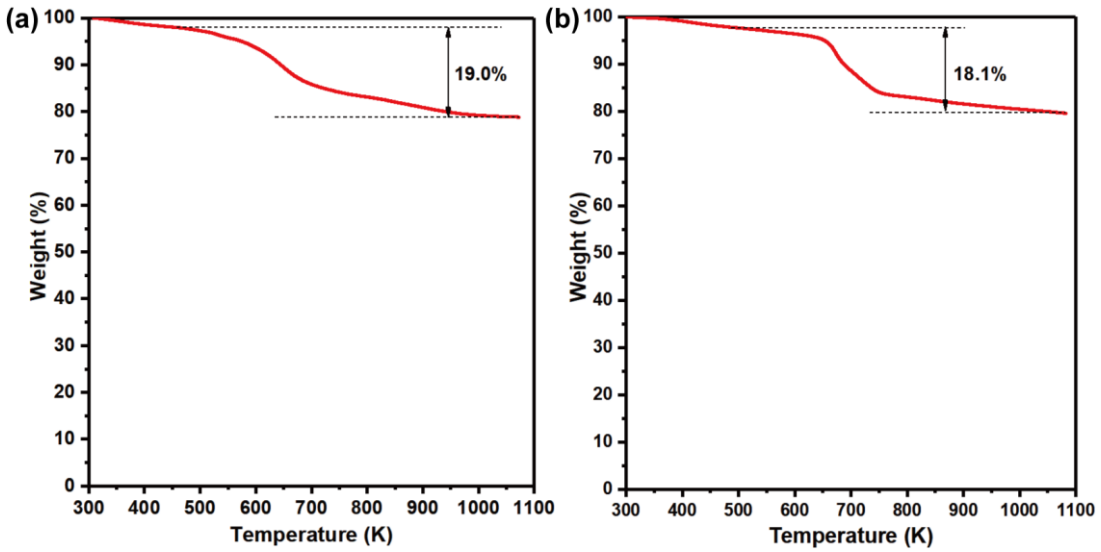

Fig. S7 Thermogravimetric analysis (TGA) curves of as-synthesized ZSM-5-NPr_2-C_6-(50) (a) and ZSM-5-C-(50) (b).

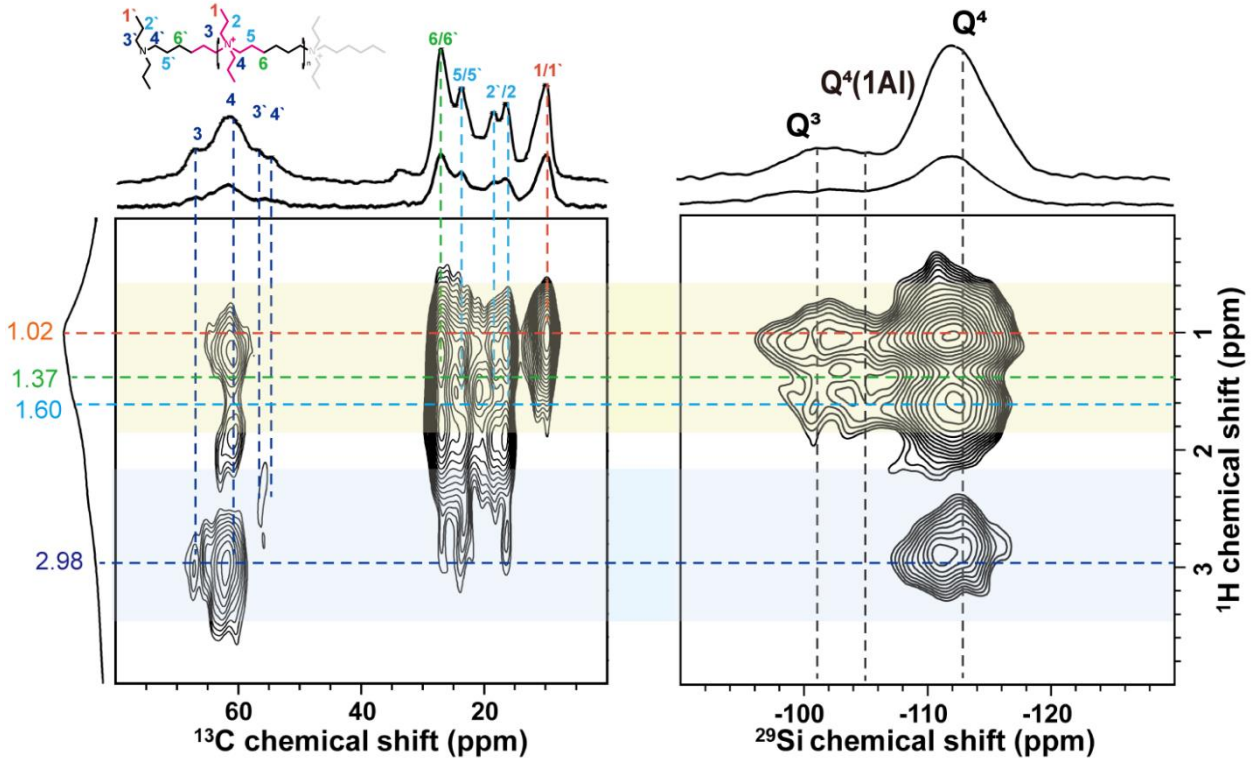

Fig. S8 Two-dimension (2D) ^{1}H-^{13}C (left) and ^{1}H-^{29}Si (right) heteronuclear correlation (HETCOR) MAS NMR spectra of ZSM-5-NPr_2-C_6-(100). One-dimensional ^{13}C CP MAS, ^{29}Si CP MAS and ^{1}H MAS NMR spectra are shown on the axes. The 2D correlated signal intensities associated with Q^3 and Q^4 species at –101 ppm, –105 ppm and –113 ppm and $–CH_3$ (1/1`) and $–CH_2–$ (2/2`, 5/5` and 6/6`) ^{1}H moieties at 1.02–1.60 ppm demonstrate that the -NPr_2-C_6- has been occluded in the crystallization and there are strong interactions between framework aluminosilicate species and the OSDA. The ^{1}H NMR resonances at ca. 2.98 ppm correspond to $–N^+CH_2–$ (3/3` and 4/4`), which are correlated with the Q^4 = $[Si(OSi)_4]$ groups in the zeolite framework. Importantly, there is an absence of 2D correlated signal intensity between ^{29}Si framework moieties and ^{1}H signals at 2.98 ppm associated with $–N^+CH_2–$ (3/3` and 4/4`), indicating that $–N^+CH_2–$ only serves a structure-oriented function.

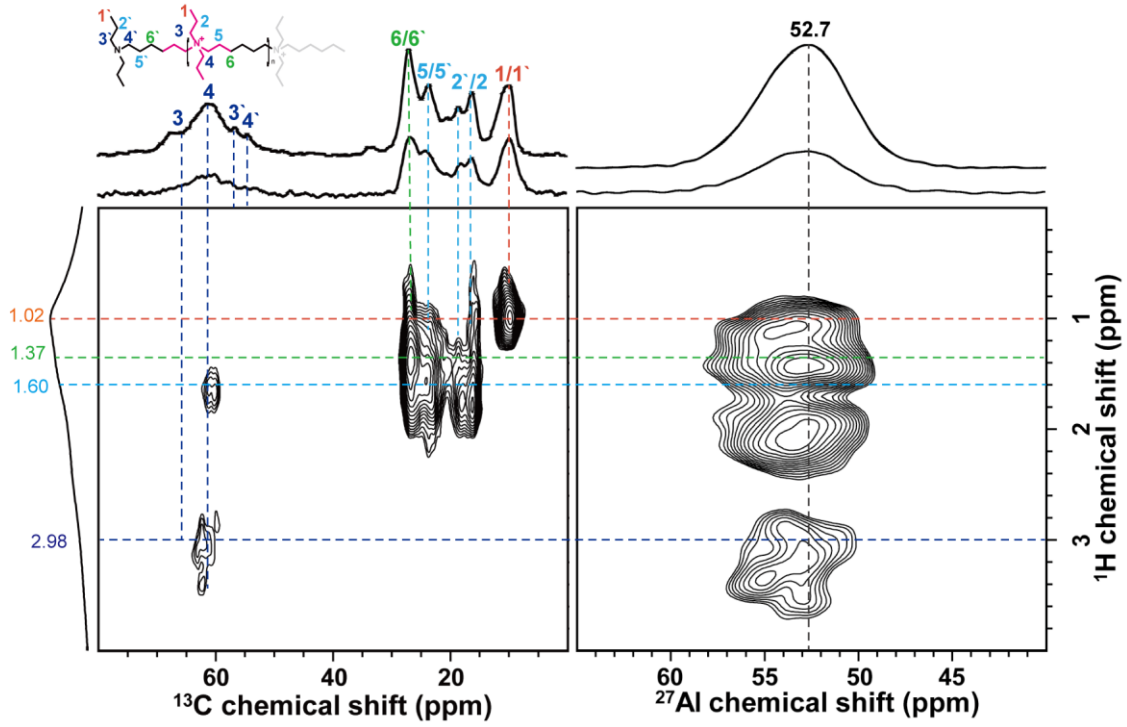

Fig. S9 ^{1}H-^{13}C (left) and ^{1}H-^{27}Al (right) HETCOR MAS NMR spectra of ZSM-5-NPr$_2$-C$_6$-(50). One-dimensional ^{13}C CP MAS, ^{29}Si CP MAS and ^{1}H MAS NMR spectra are shown on the axes.

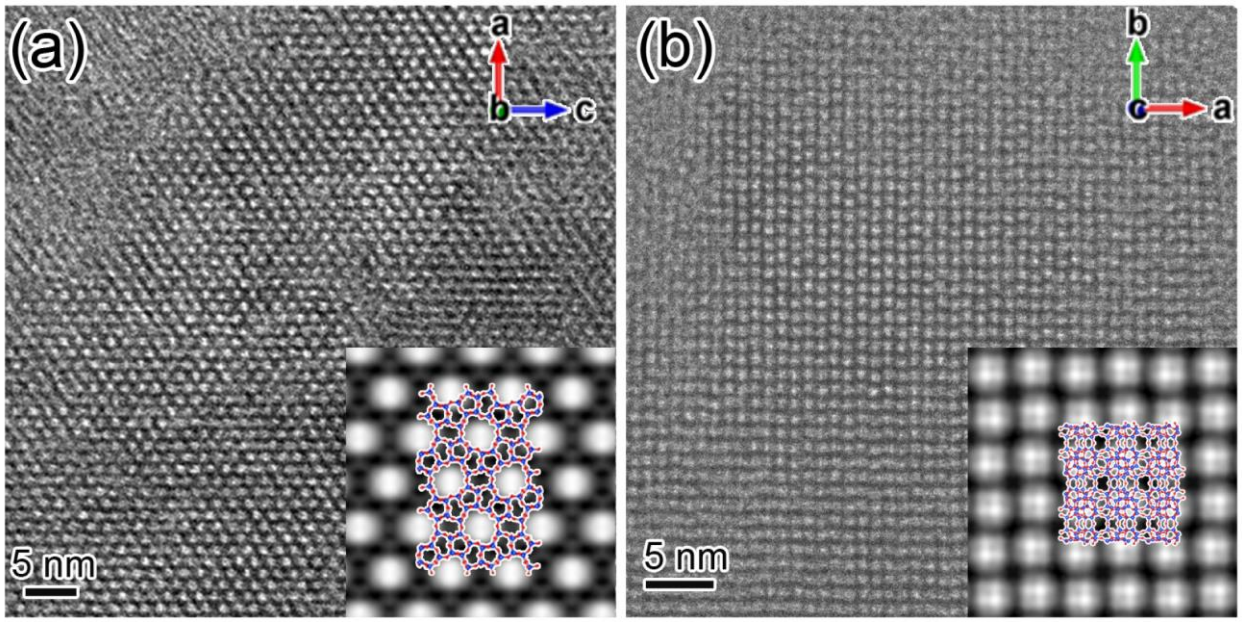

Fig. S10 HRTEM images of calcined samples taken from the ***b***-axis (a) and the ***c***-axis (b) of the ZSM-5-NPr_2-C_6-(50) particle. The averaged HRTEM images and structural models are illustrated in the lower right corner after Fourier transformation using the crystallographic image processing software CRISP[4] with only translational symmetry applied (plane group p1).

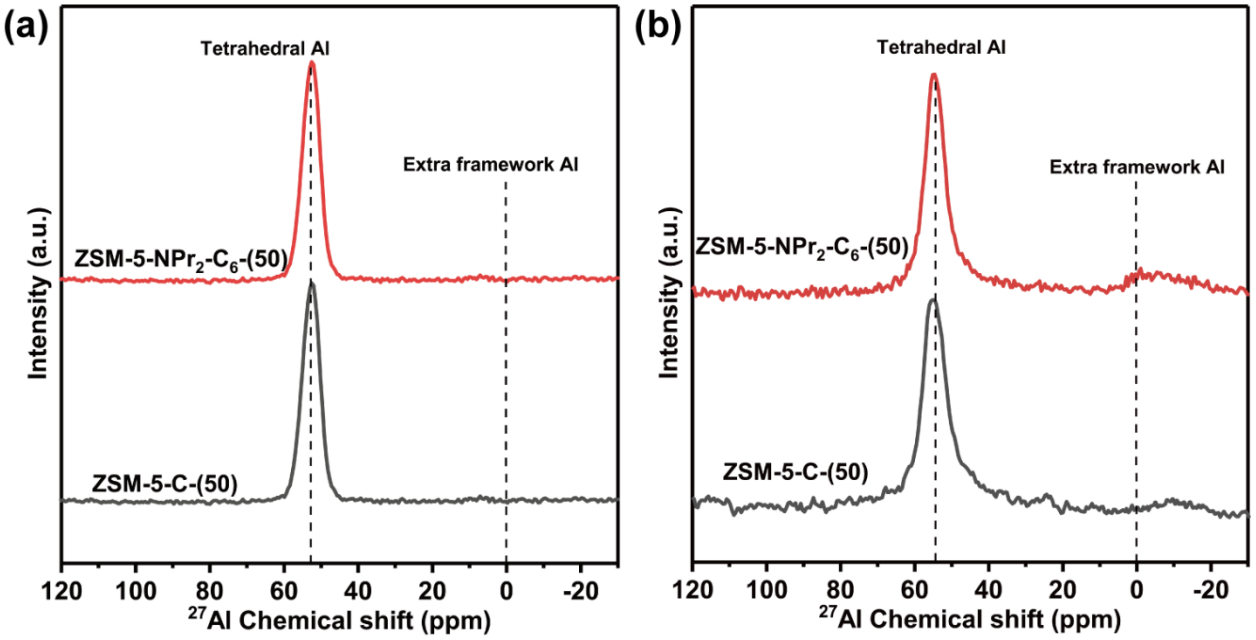

Fig. S11 ^{27}Al MAS NMR spectra of as-synthesized (a) and calcined (b) samples for ZSM-5-C-(50) and ZSM-5-NPr$_2$-C$_6$-(50).

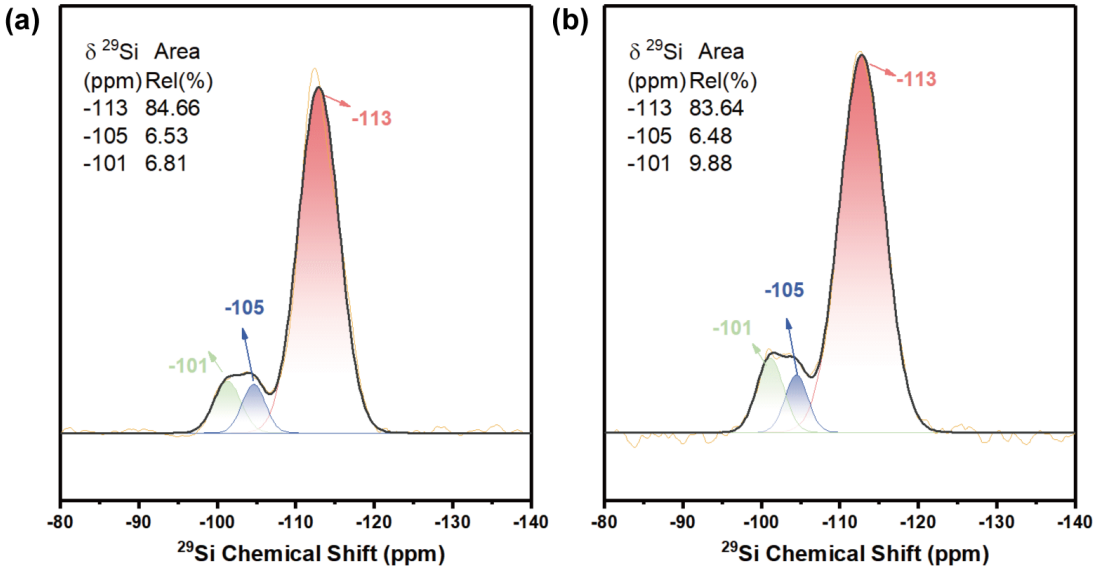

Fig. S12 ^{29}Si MAS NMR spectra of as-synthesized ZSM-5-C-(50) (a) and ZSM-5-NPr_2-C_6-(50) (b). The chemical shift for each component after deconvolution of the profile and the relevant proportion are shown in the insets.

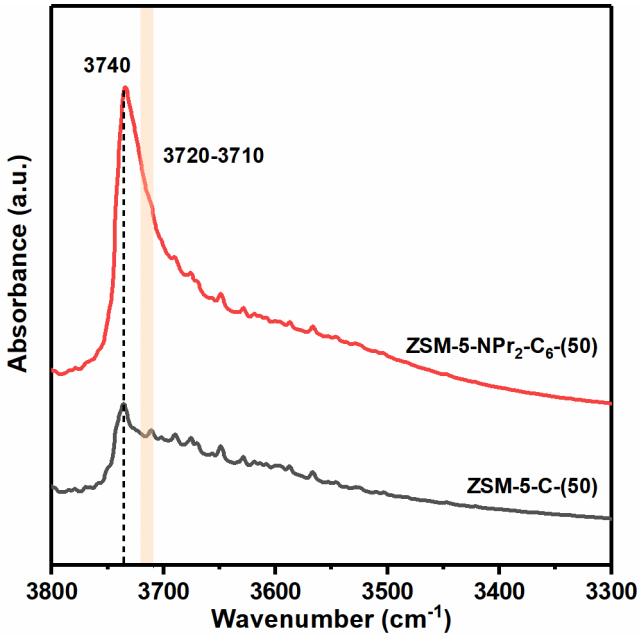

Fig. S13 FT-IR spectra in the region of hydroxyl stretching vibration for the proton type ZSM-5-C-(50) and ZSM-5-NPr$_2$-C$_6$-(50) samples.

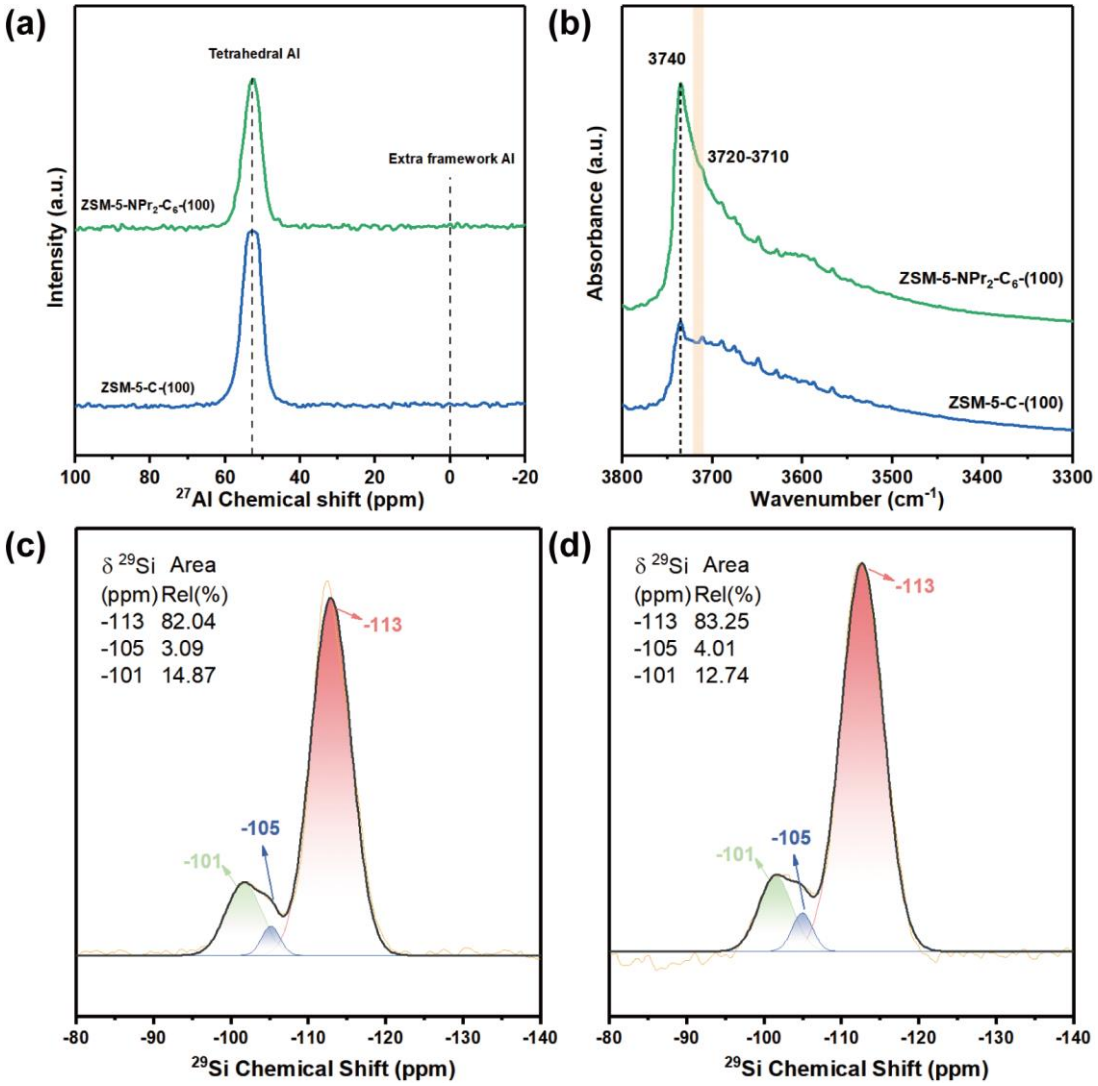

Fig. S14 ^{27}Al MAS NMR spectra (a) of as-synthesized ZSM-5-(100) and ZSM-5-NPr$_2$-C$_6$-(100), FT-IR spectra (b) in the region of hydroxyl stretching vibration for HZSM-5 samples, ^{29}Si MAS NMR spectra of ZSM-5-C-(100) (c) and ZSM-5-NPr$_2$-C$_6$-(100) (d).

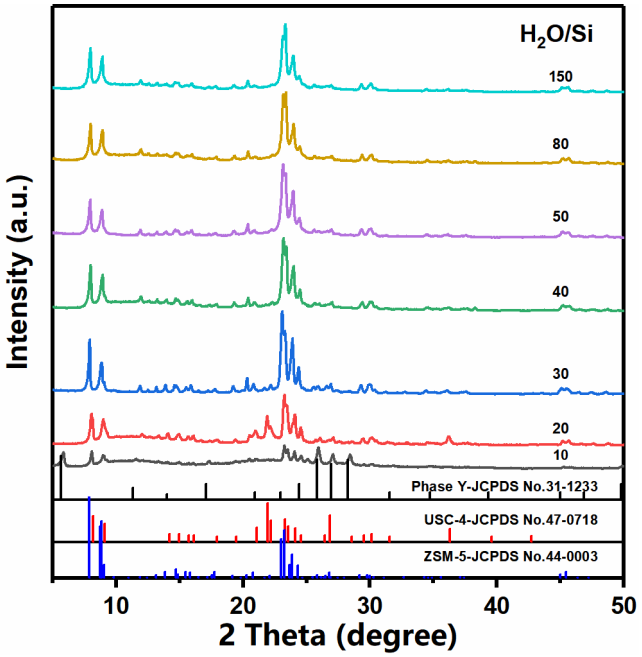

Fig. S15 XRD patterns of products synthesized from reaction mixtures of 1 SiO_2: 0.01 Al_2O_3: 0.30 -NPr_2-C_6-: 0.15 NaOH: 10–150 H_2O: 4 EtOH.

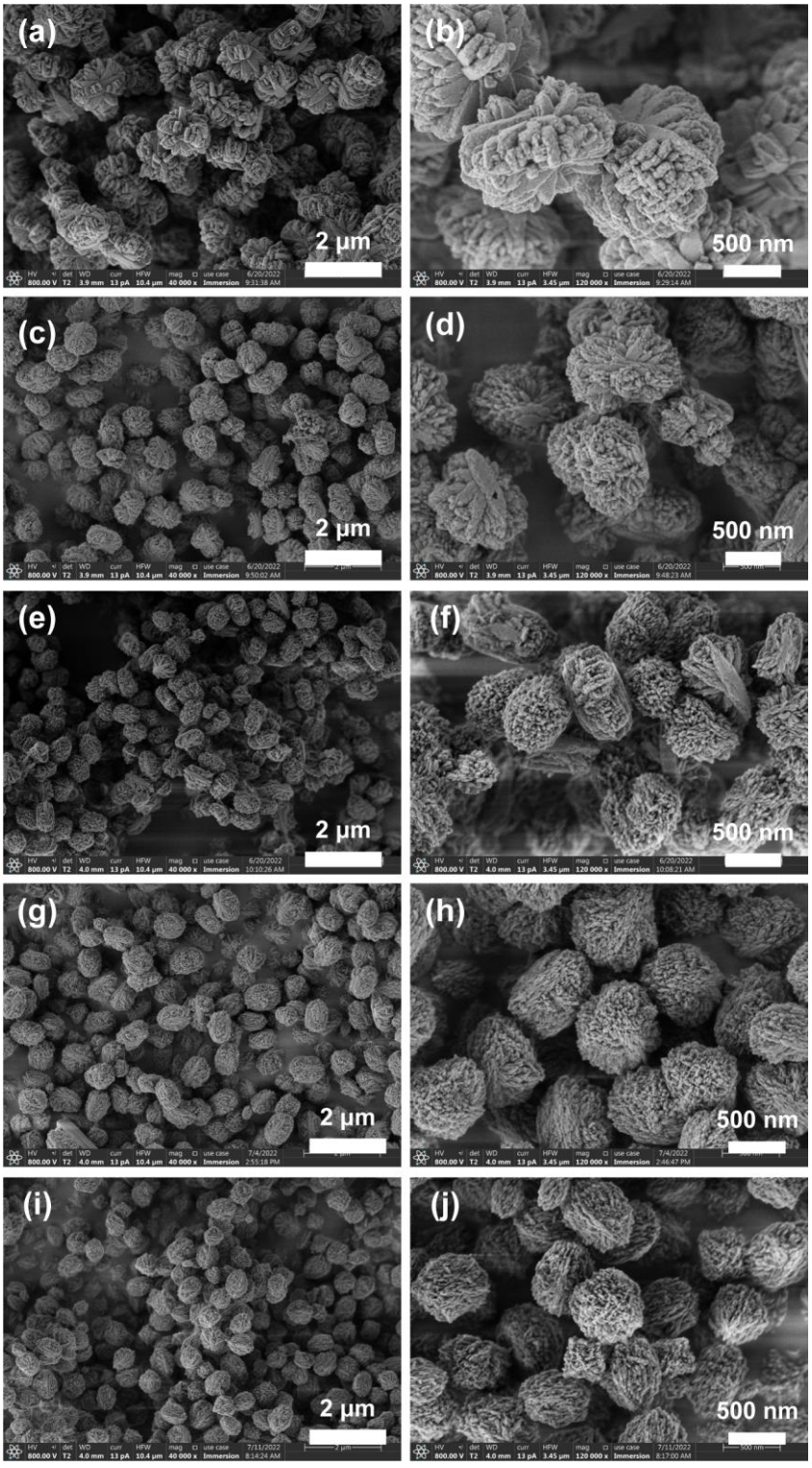

Fig. S16 FE-SEM micrographs of products synthesized from reaction mixtures of 1 SiO_2: 0.01 Al_2O_3: 0.30 -NPr_2-C_6-: 0.15 NaOH: 10–150 H_2O: 4 EtOH at H_2O/SiO_2 of 30 (a-b), 40 (c, d), 50 (e, f), 80 (g, h), and 150 (i, j).

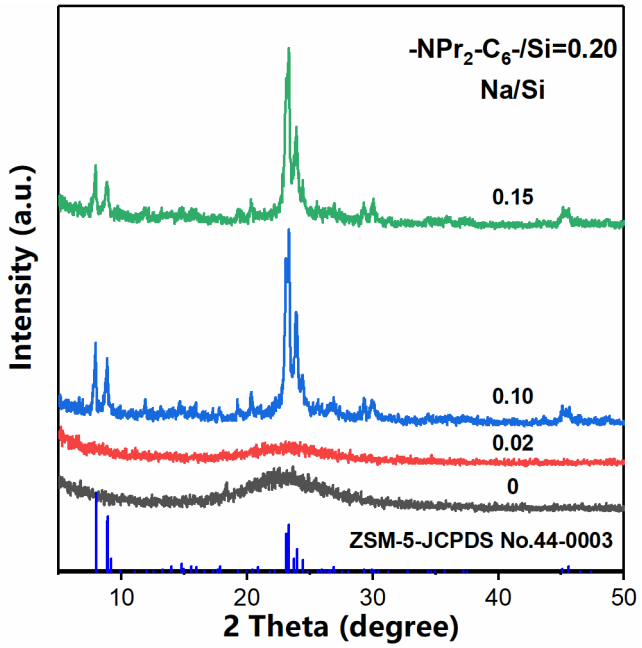

Fig. S17 XRD patterns of products synthesized from reaction mixtures of 1 SiO_2: 0.01 Al_2O_3: 0.20 -NPr_2-C_6-: 0–0.15 NaOH: 150 H_2O: 4 EtOH.

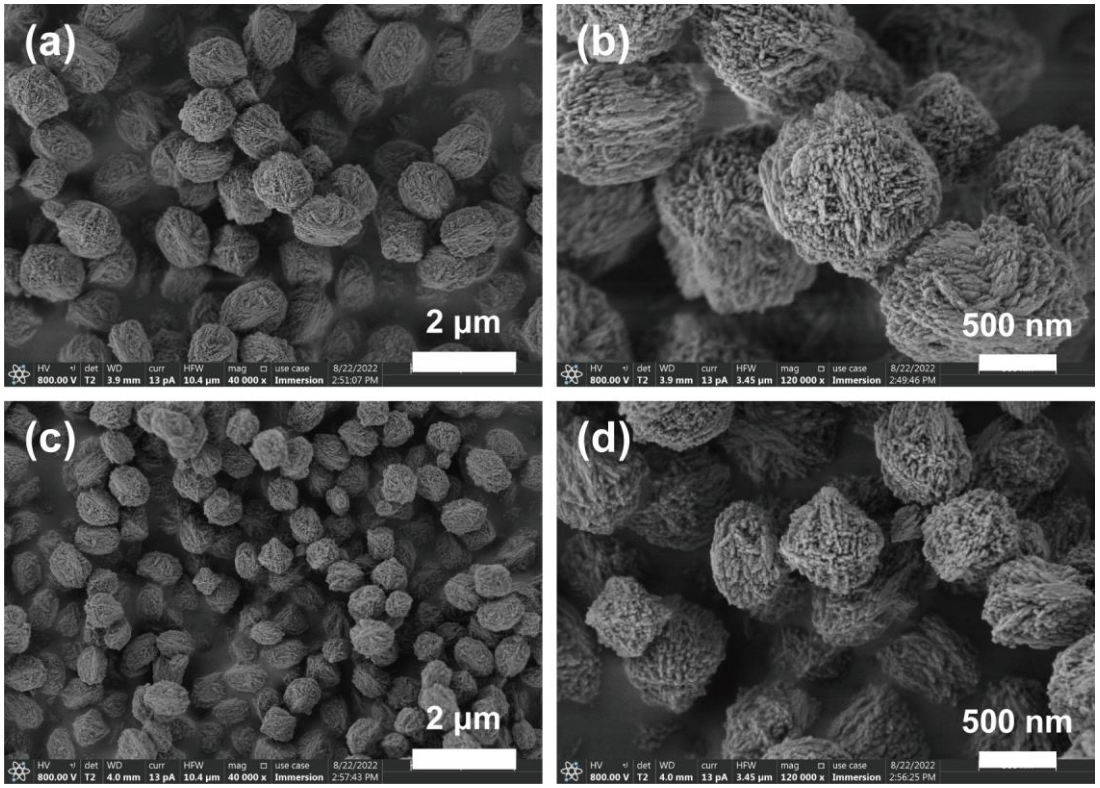

Fig. S18 FE-SEM micrographs of products synthesized from reaction mixtures of 1 SiO_2: 0.01 Al_2O_3: 0.20 -NPr_2-C_6-: 0–0.15 NaOH: 150 H_2O: 4 EtOH at Na^+/Si of 0.10 (a, b), 0.15 (c, d).

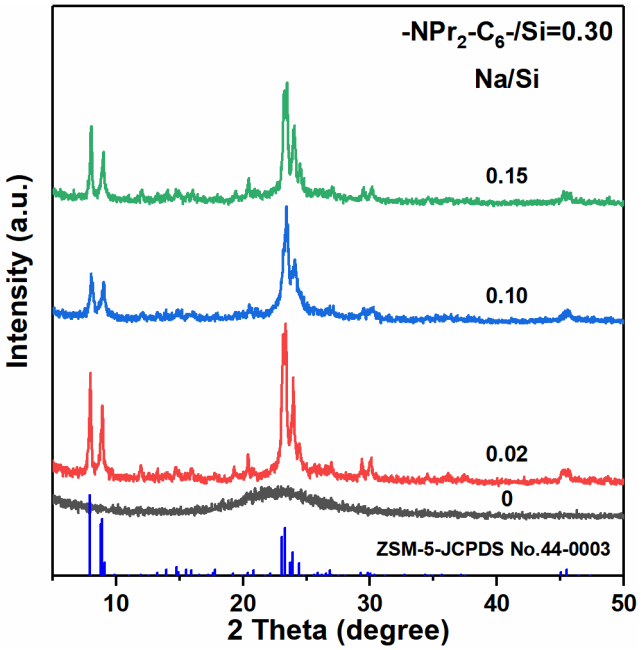

Fig. S19 XRD patterns of products synthesized from reaction mixtures of 1 SiO_2: 0.01 Al_2O_3: 0.30 -NPr_2-C_6-: 0–0.15 NaOH: 150 H_2O: 4 EtOH.

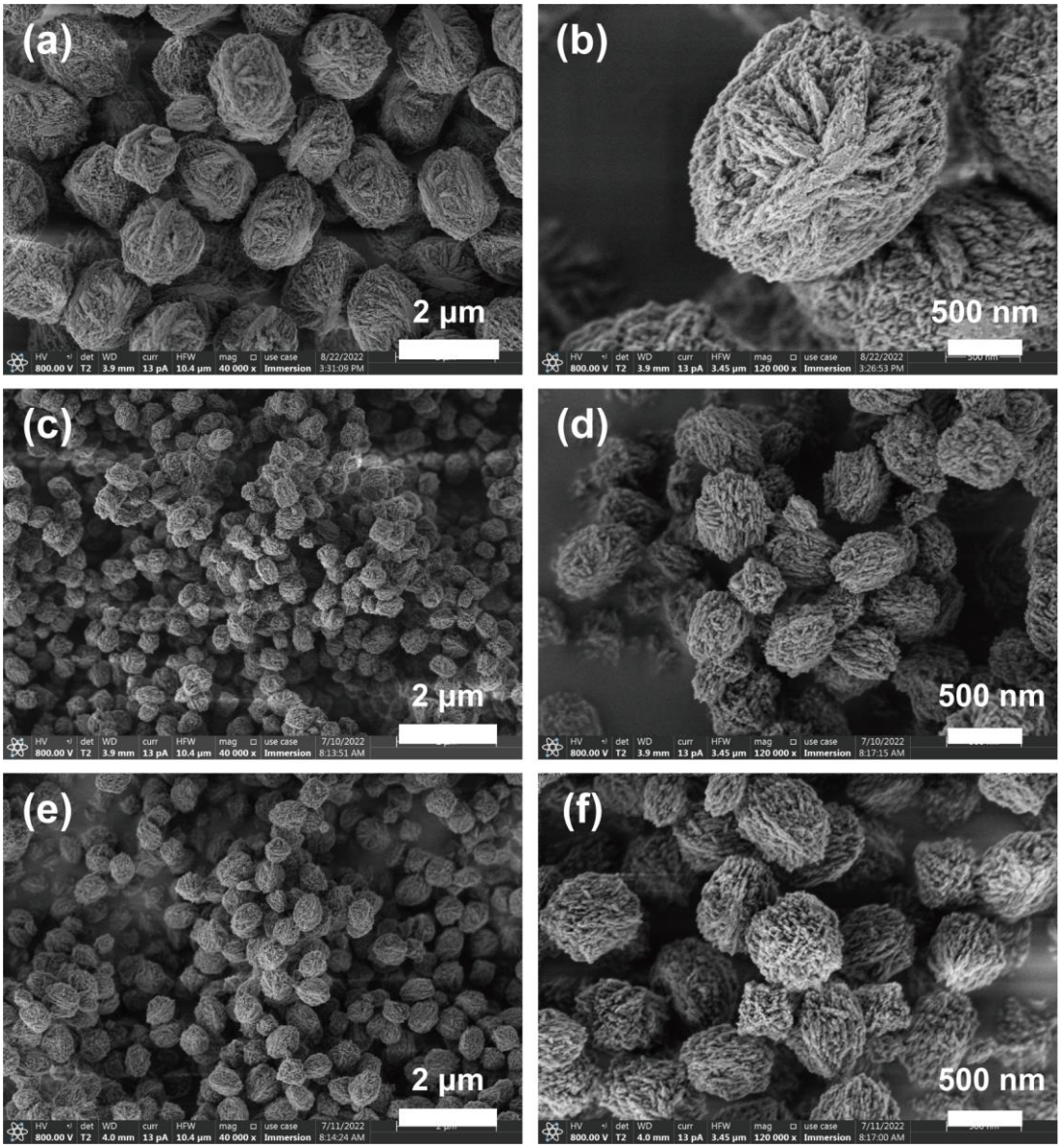

Fig. S20 FE-SEM micrographs of products synthesized from reaction mixtures of 1 SiO_2: 0.01 Al_2O_3: 0.30 -NPr_2-C_6-: 0–0.15 NaOH: 150 H_2O: 4 EtOH at Na^+/Si of 0.02 (a, b), 0.10 (c, d), 0.15 (e, f).

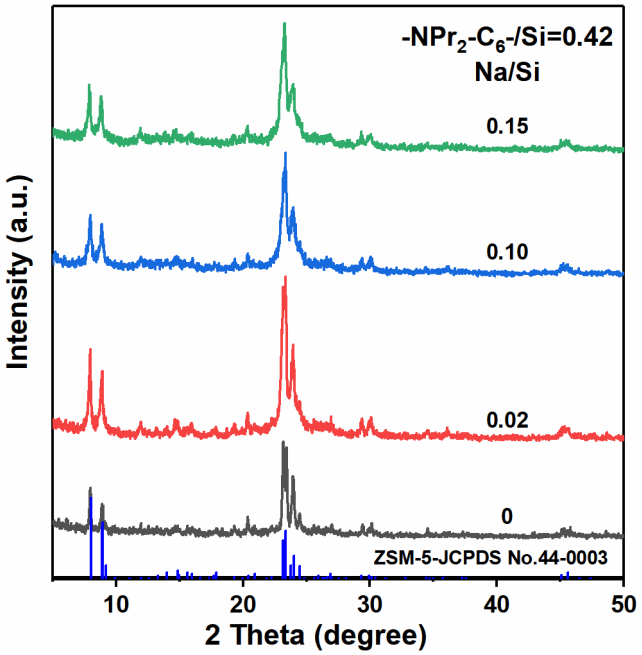

Fig. S21 XRD patterns of products synthesized from reaction mixtures of 1 SiO_2: 0.01 Al_2O_3: 0.42 -NPr_2-C_6-: 0–0.15 NaOH: 150 H_2O: 4 EtOH.

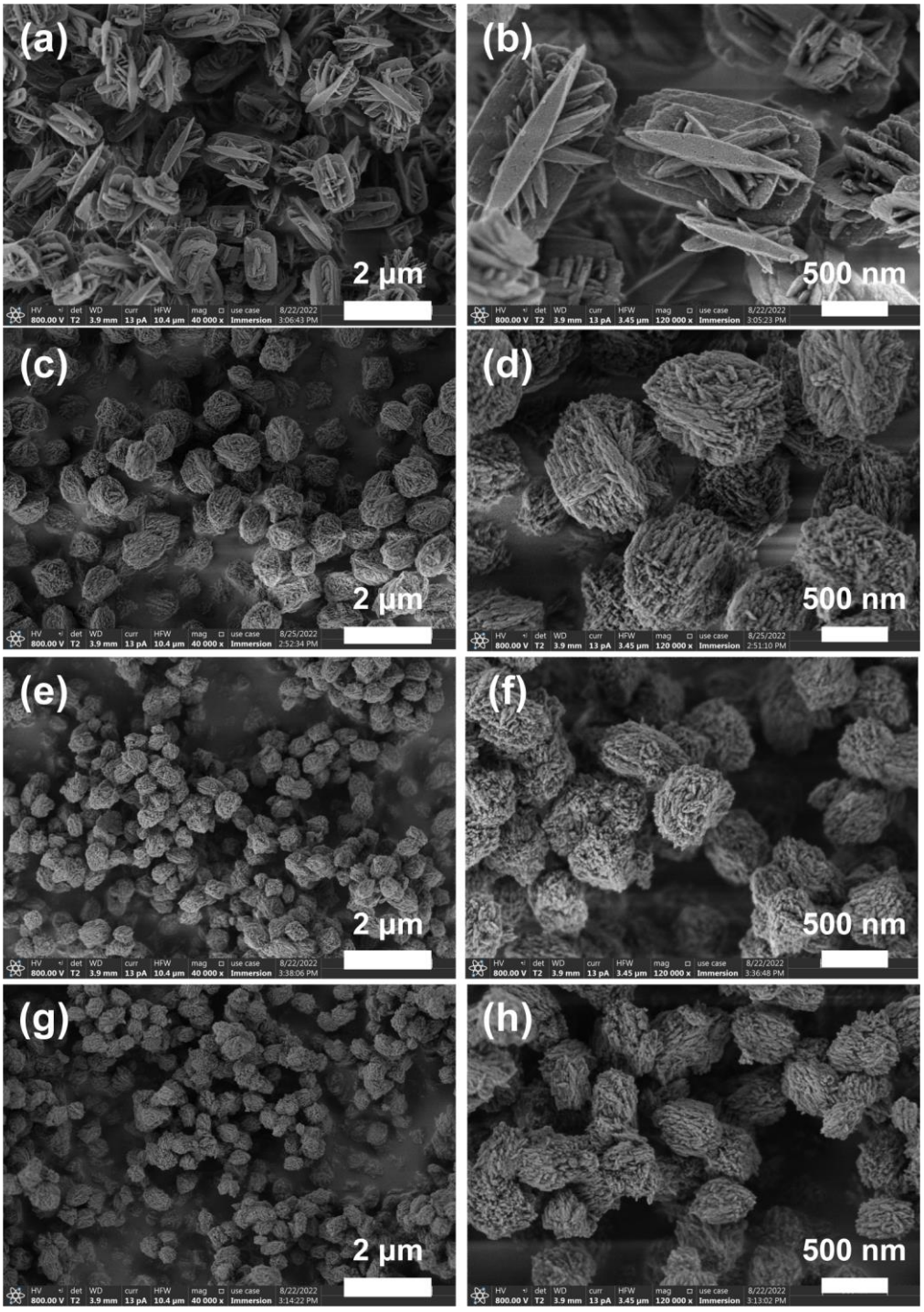

Fig. S22 FE-SEM micrographs of products synthesized from reaction mixtures of 1 SiO_2: 0.01 Al_2O_3: 0.42 -NPr_2-C_6-: 0–0.15 NaOH: 150 H_2O: 4 EtOH at Na^+/Si of 0 (a, b), 0.02 (c, d), 0.10 (e, f), 0.15 (g, h).

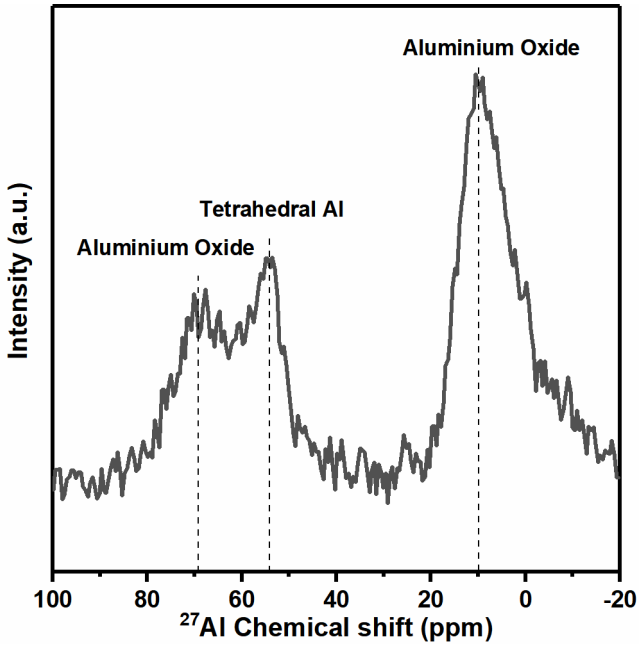

Fig. S23 ^{27}Al MAS-NMR spectra of calcined product synthesized from the reaction mixture of 1 SiO_2: 0.01 Al_2O_3: 0.42 -NPr_2-C_6-: 150 H_2O: 4 EtOH.

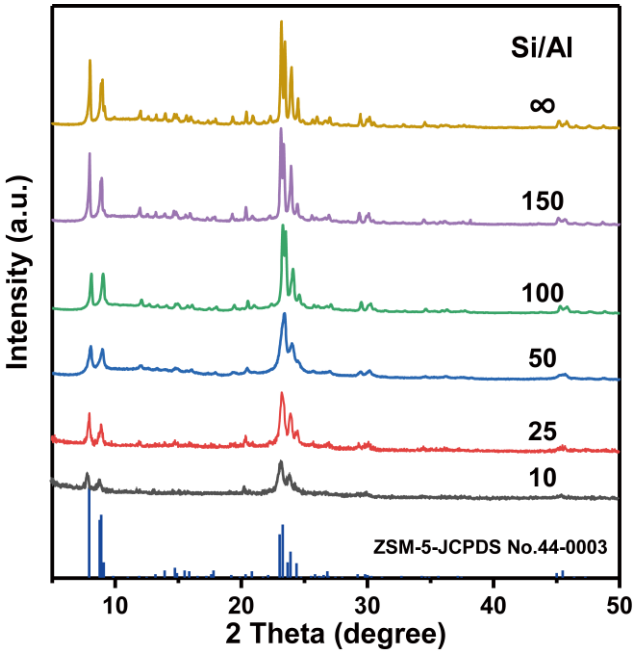

Fig. S24 XRD patterns of products synthesized from reaction mixtures of 1 SiO_2: 0–0.05 Al_2O_3: 0.20 -NPr_2-C_6-: 0.15 NaOH: 150 H_2O: 4 EtOH, with varied Si/Al ratios.

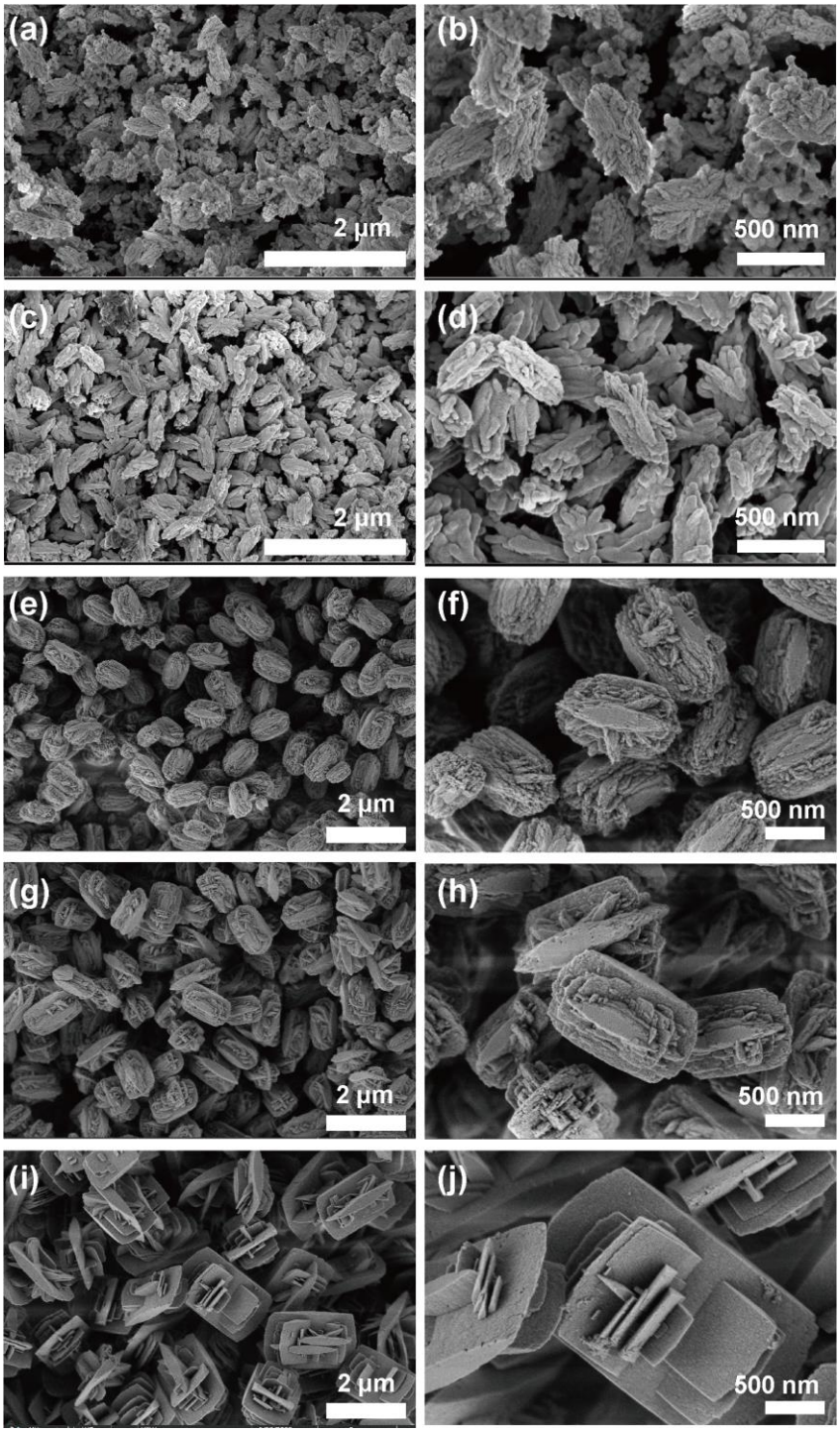

Fig. S25 FE-SEM micrographs of products synthesized from reaction mixtures of 1 SiO_2: 0–0.005 Al_2O_3: 0.20 -NPr_2-C_6-: 0.15 NaOH: 150 H_2O: 4 EtOH with Si/Al of 10 (a, b), 25 (c, d), 100 (e, f), 150 (g, h), ∞ (i, j).

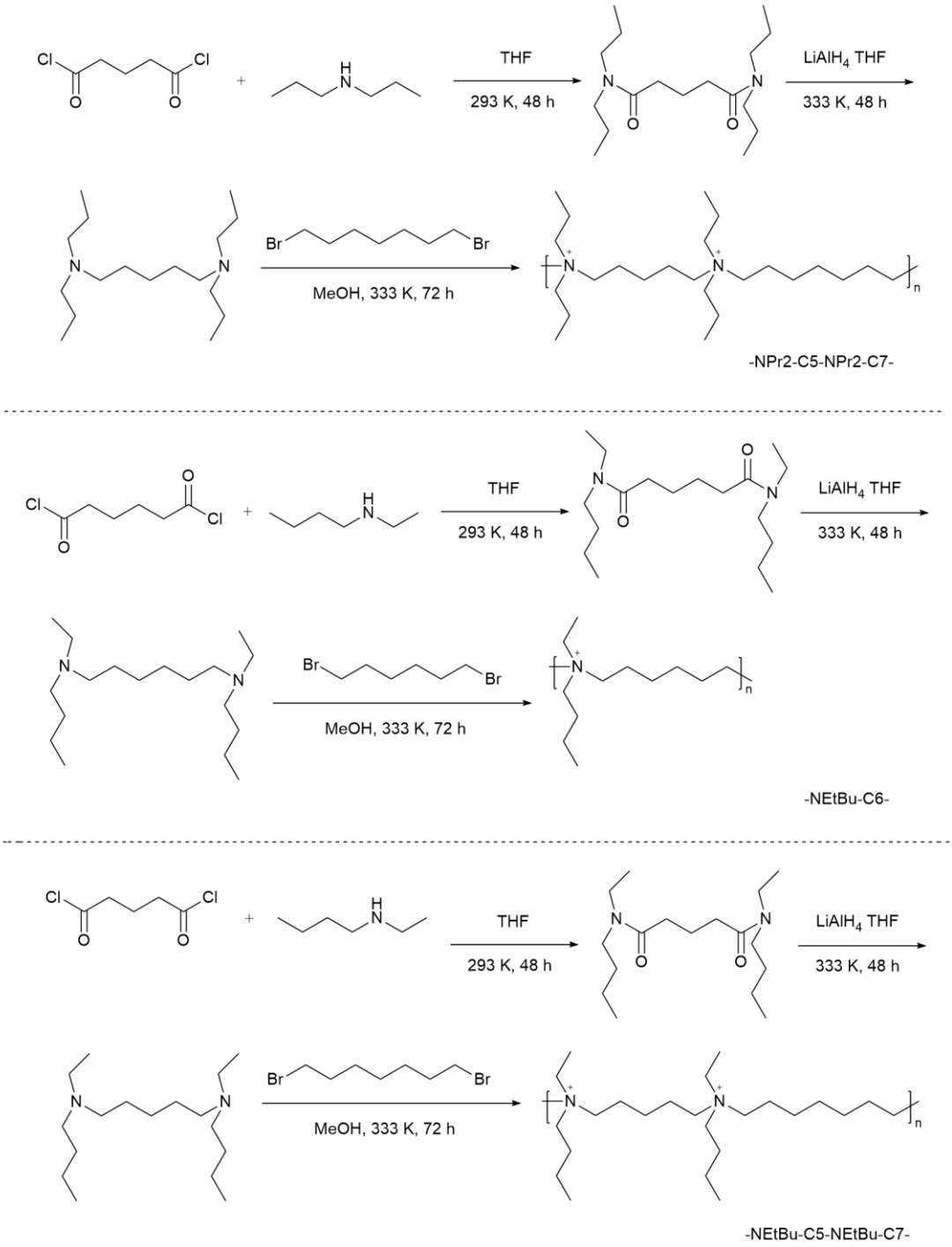

Fig. S26 Synthesis of poly-quaternary ammonium OSDAs (-NPr_2-C_5-NPr_2-C_7-, -NEtBu-C_6-, and -NEtBu-C_5-NEtBu-C_7-).

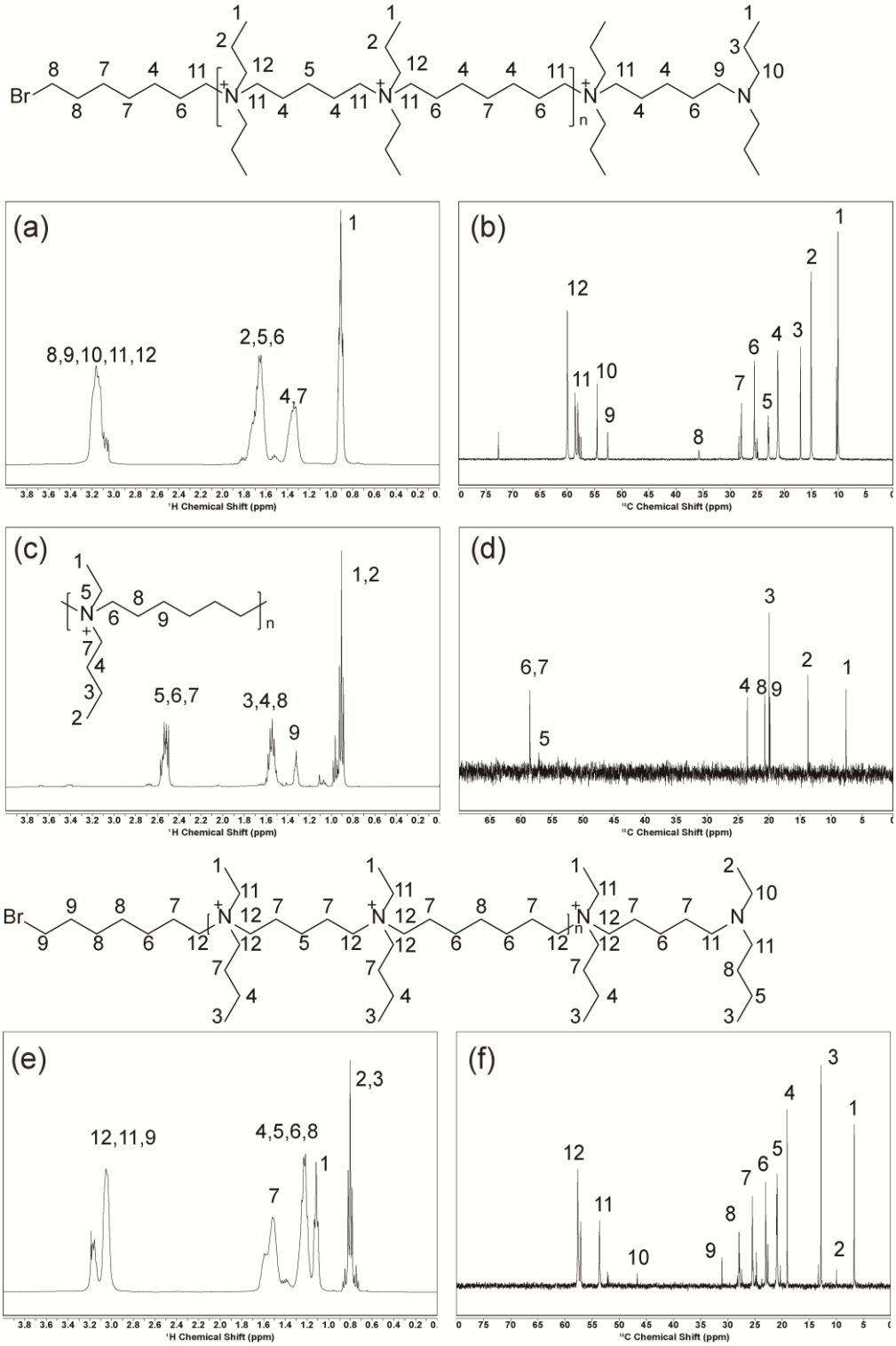

Fig. S27 Solution-state ^{1}H NMR and ^{13}C NMR spectra of -NPr_2-C_5-NPr_2-C_7- (a, b), -NEtBu-C_6- (c, d), -NEtBu-C_5-NEtBu-C_7- (e, f) in D_2O. The numbers denote the corresponding position of protons in the corresponding OSDAs, as illustrated above the resonance peaks.

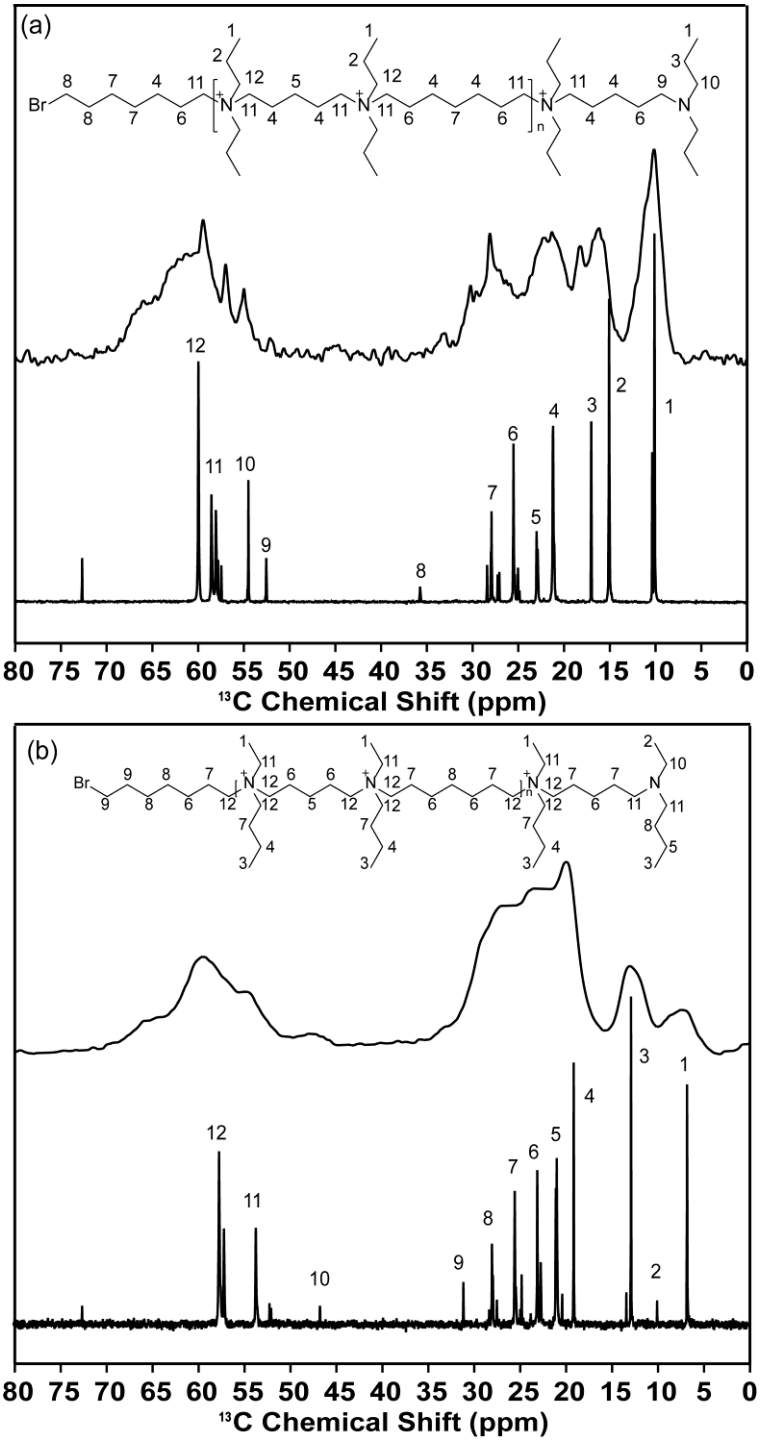

Fig. S28 Solid state ^{13}C CP MAS NMR spectra of as-made ZSM-5-NPr_2-C_5-NPr_2-C_7-(50) (a) and ZSM-5-NEtBu-C_5-NEtBu-C_7-(50) (b) zeolite (top) and liquid ^{13}C NMR spectra in D_2O of pristine -NPr_2-C_5-NPr_2-C_7- (a) and -NEtBu-C_5-NEtBu-C_7- (b), respectively (bottom). The resonances of C atoms in the as-made ZSM-5 samples are consistent with the resonances of the pristine OSDAs, confirming the integrity of the OSDAs during the crystallization process.

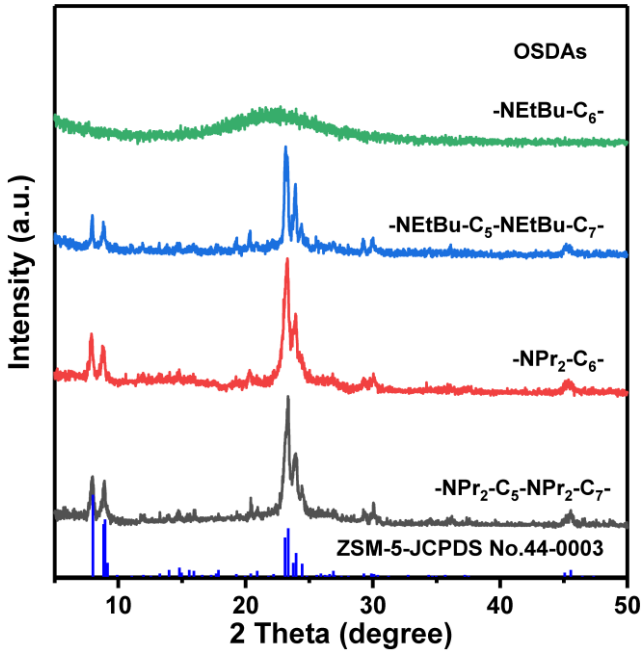

Fig. S29 XRD patterns of products synthesized from reaction mixtures of 1 SiO_2: 0.01 Al_2O_3: 0.20 -NEtBu-C_6-: 0.15 NaOH: 150 H_2O: 4 EtOH and 1 SiO_2: 0.01 Al_2O_3: 0.10 OSDAs: 0.15 NaOH: 150 H_2O: 4 EtOH (OSDAs = -NPr_2-C_5-NPr_2-C_7-, -NEtBu-C_5-NEtBu-C_7-), with fixed N^+/Si ratio of 0.2.

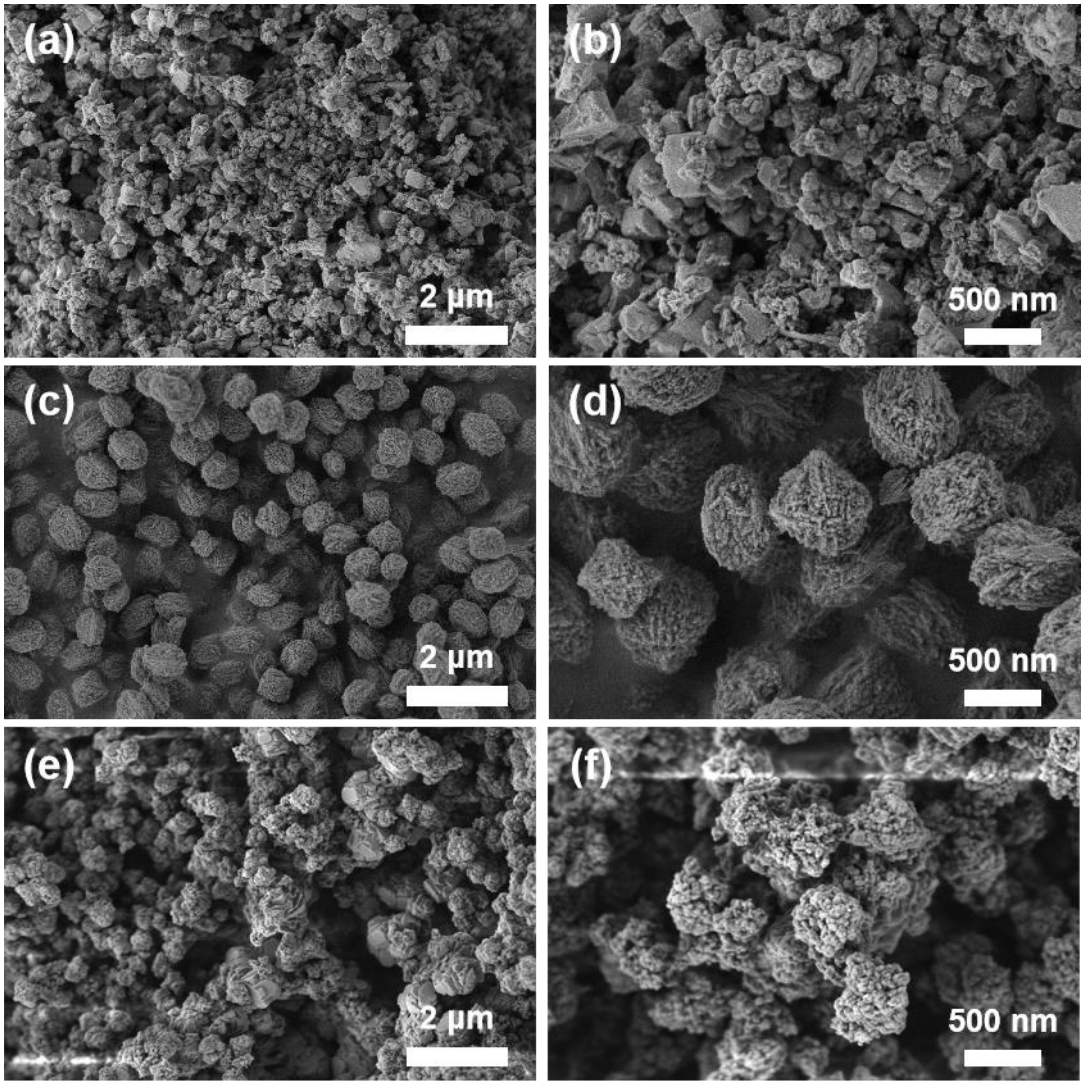

Fig. S30 FE-SEM micrographs of products synthesized from reaction mixtures of 1 SiO_2: 0.01 Al_2O_3: 0.20 -NEtBu-C_6-: 0.15 NaOH: 150 H_2O: 4 EtOH and 1 SiO_2: 0.01 Al_2O_3: 0.10 OSDAs: 0.15 NaOH: 150 H_2O: 4 EtOH (OSDAs: -NPr_2-C_5-NPr_2-C_7-, -NEtBu-C_5-NEtBu-C_7-), with fixed N^+/Si ratio of 0.2. OSDAs: -NPr_2-C_5-NPr_2-C_7- (a, b), -NPr_2-C_6- (c, d), -NEtBu-C_5-NEtBu-C_7- (e, f). .

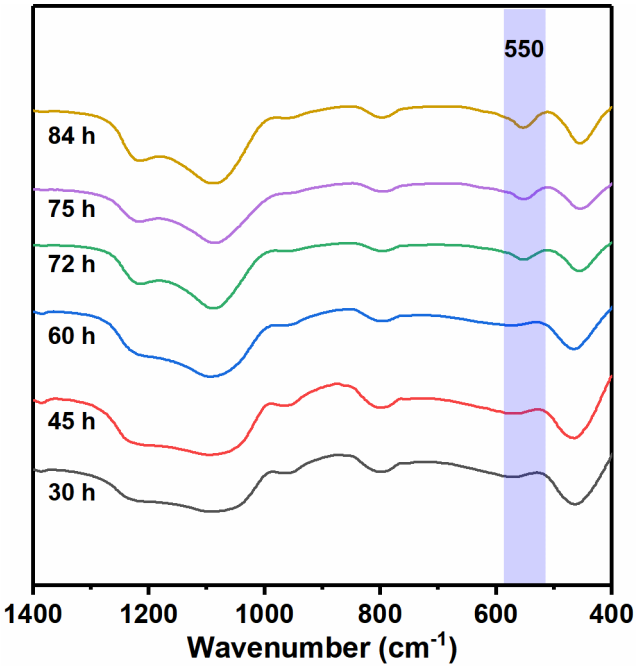

Fig. S31 FT-IR spectra for ZSM-5-NPr_2-C_6-(50) with the increasing hydrothermal heating time. The band at 550 cm^{-1} is assigned to 5-MR vibration of the **MFI** framework, which becomes visible from 72 h on and increases in intensity thereafter.

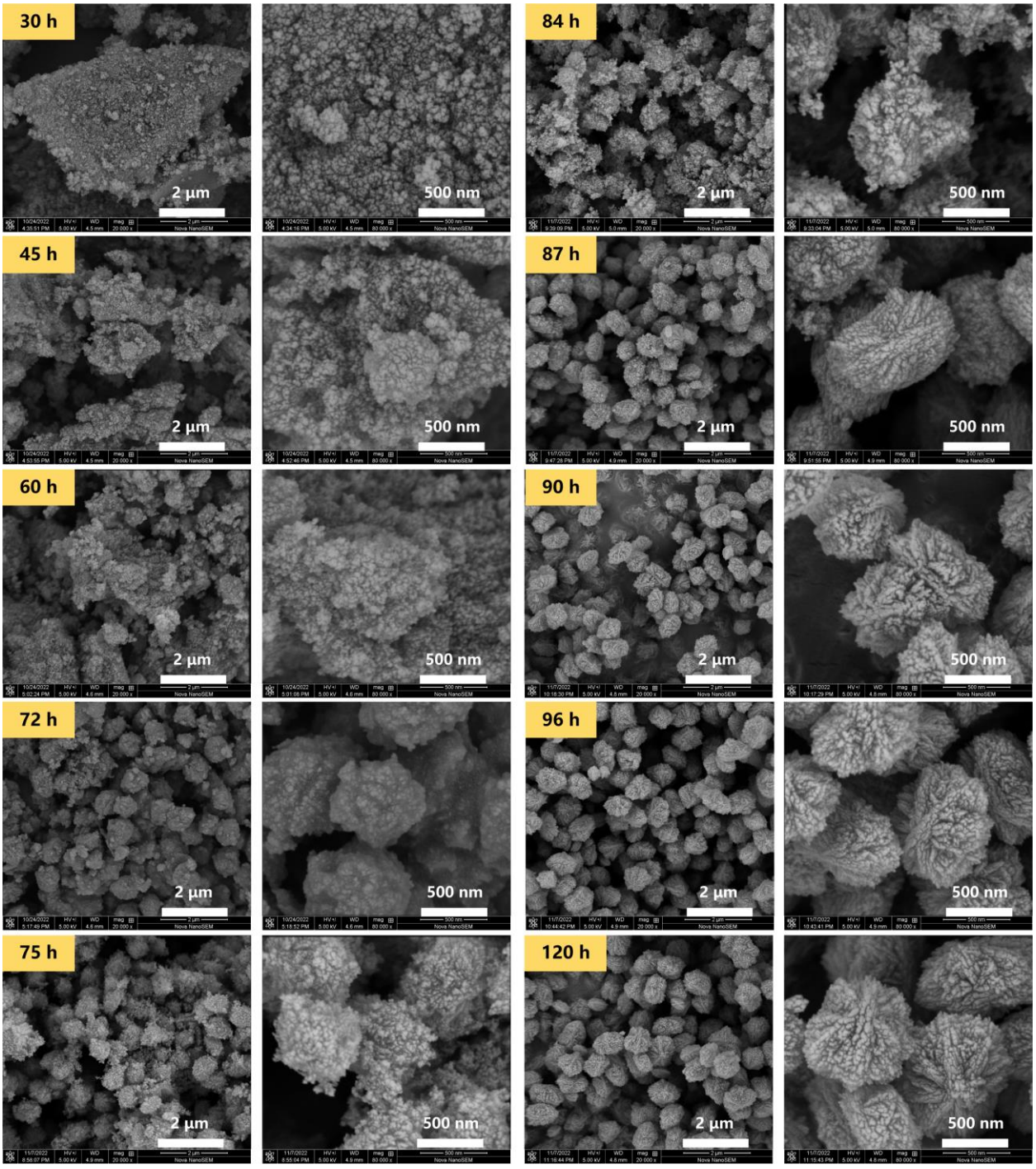

Fig. S32 Time-dependent FE-SEM micrographs for ZSM-5-NPr_2-C_6-(50) in the course of crystallization (30 h, 45 h, 60 h, 72 h, 75 h, 84 h, 87 h, 90 h, 96 h and 120 h).

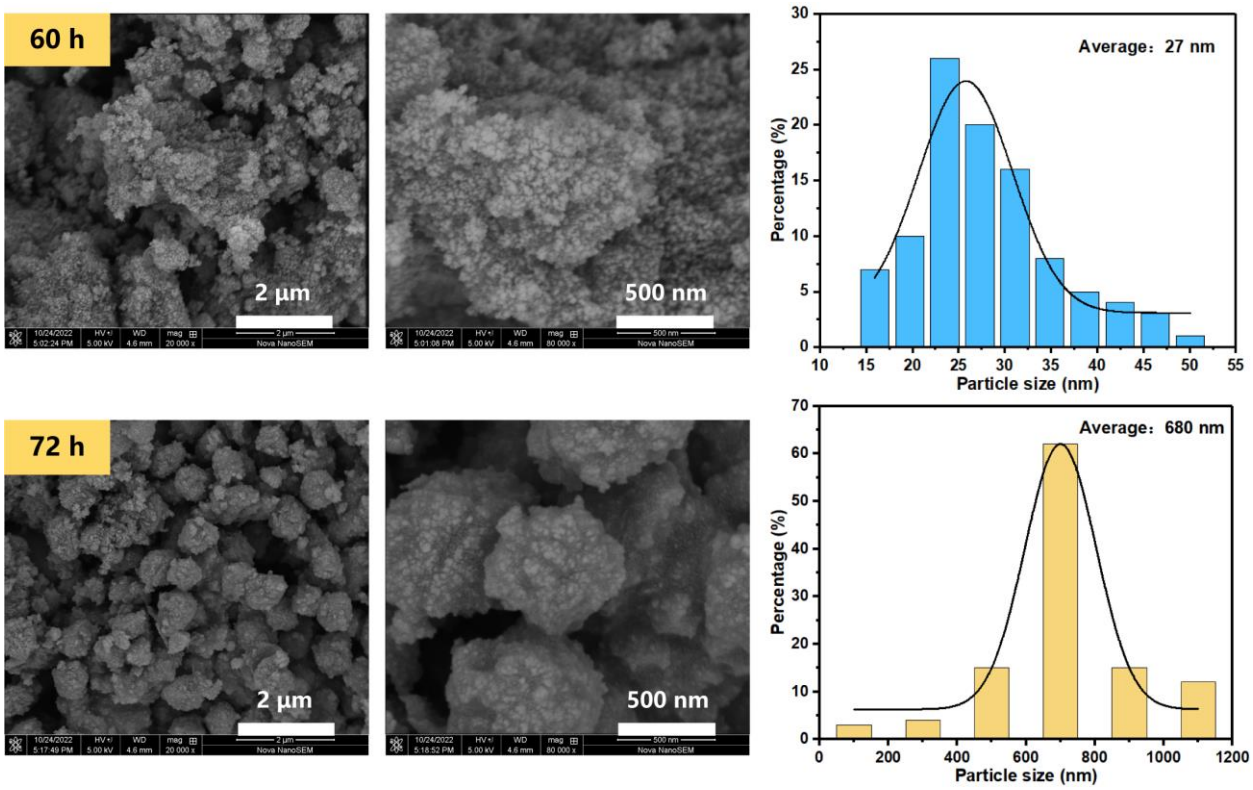

Fig. S33 FE-SEM images with intermediates (60 h, 72 h) collected during ZSM-5-NPr_2-C_6-(50) crystallization and the corresponding particle-size distributions are shown in histograms.

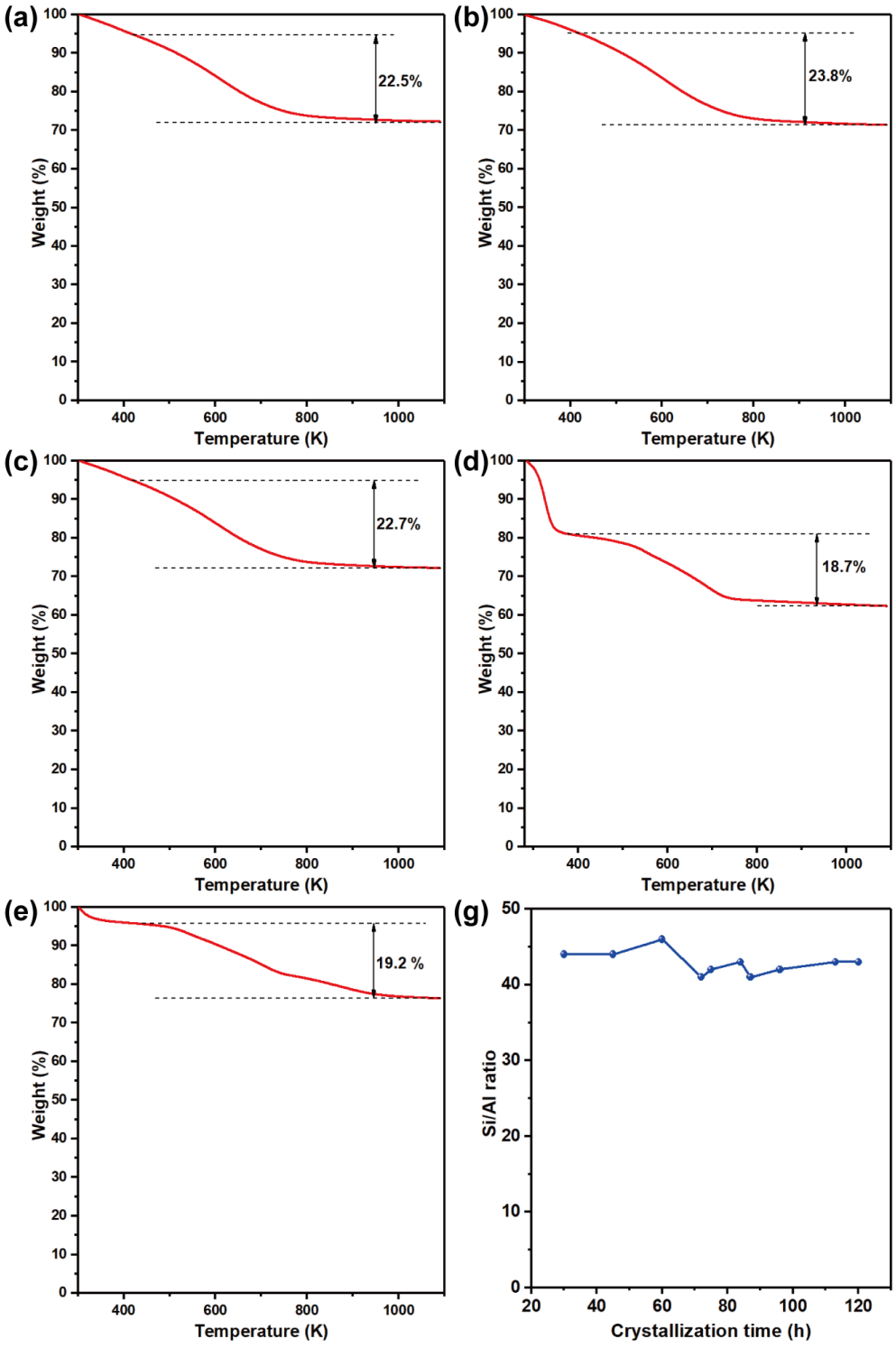

Fig. S34 TGA measurements of collected intermediate solids (a-e) and Si/Al ratio variations (g) for ZSM-5-NPr_2-C_6-(50) after hydrothermal heating for (a) 30 h, (b) 45 h, (c) 60 h, (d) 72h and (e) 87 h.

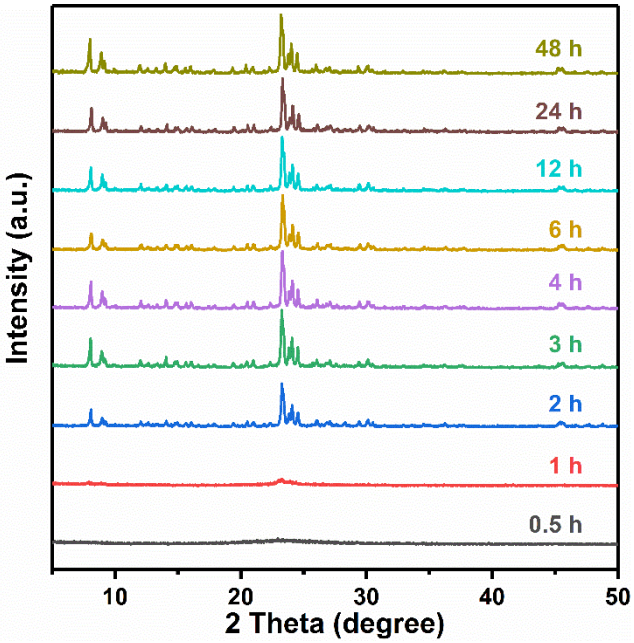

Fig. S35 Time-dependent powder XRD patterns for ZSM-5-C-(50) in the course of crystallization.

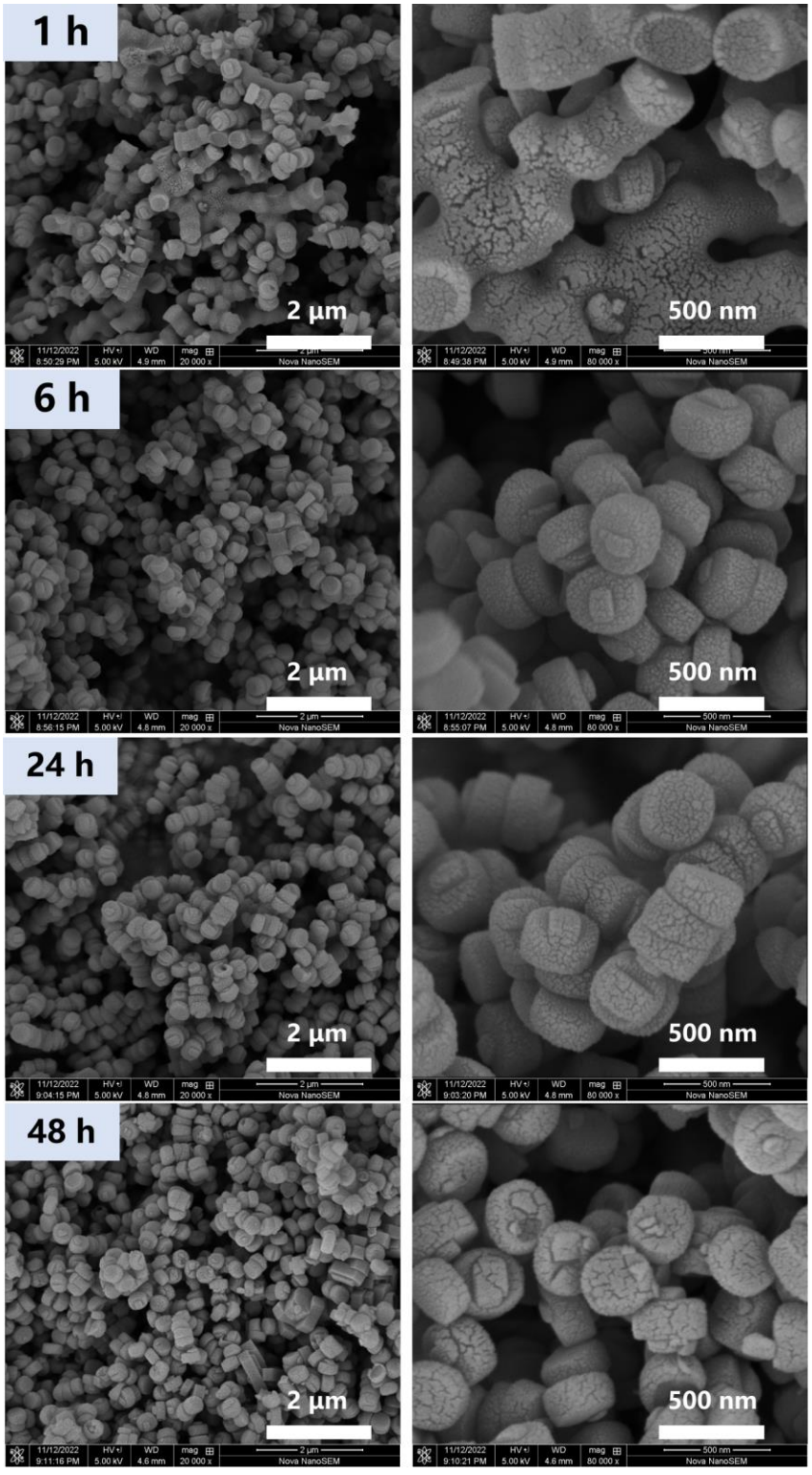

Fig. S36 Time-dependent FE-SEM micrographs for ZSM-5-C-(50) in the course of crystallization.

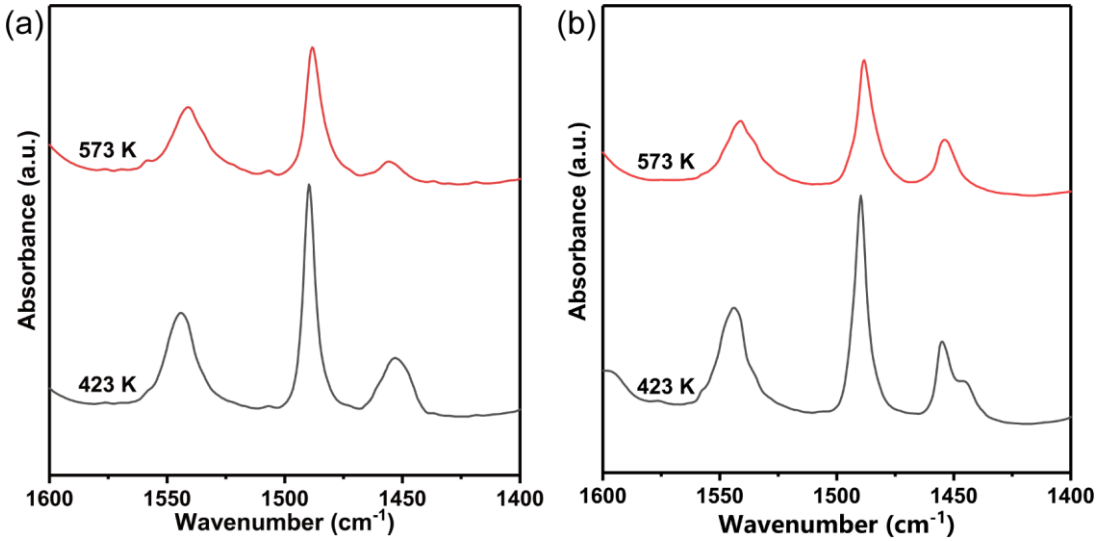

Fig. S37 Py-IR spectra of pyridine (Py) adsorbed on ZSM-5-C-(50) (a), ZSM-5-NPr_2-C_6-(50) (b) conducted at 423 K, 573 K. The number of Brønsted acid sites and Lewis acid sites were calculated from the Py-IR band area located at 1545 cm^{-1} and 1455 cm^{-1}, respectively.[3]

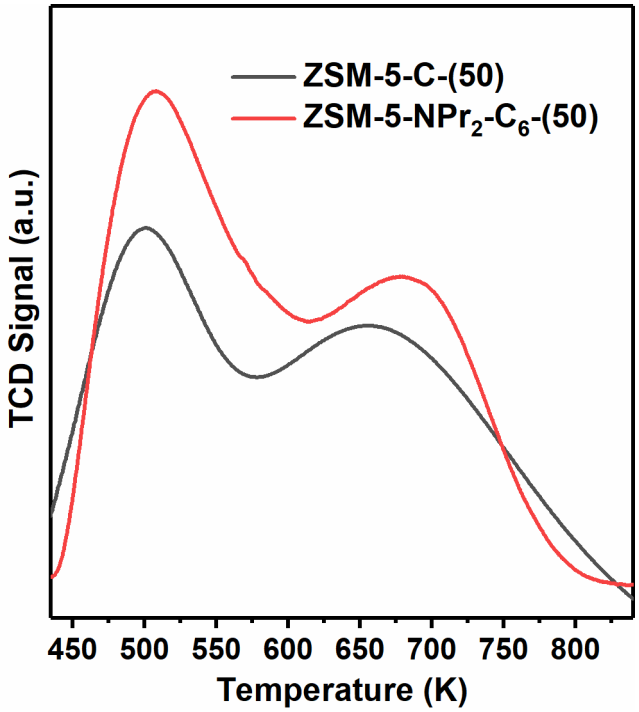

Fig. S38 NH_3-TPD curves of ZSM-5-C-(50) and ZSM-5-NPr_2-C_6-(50).

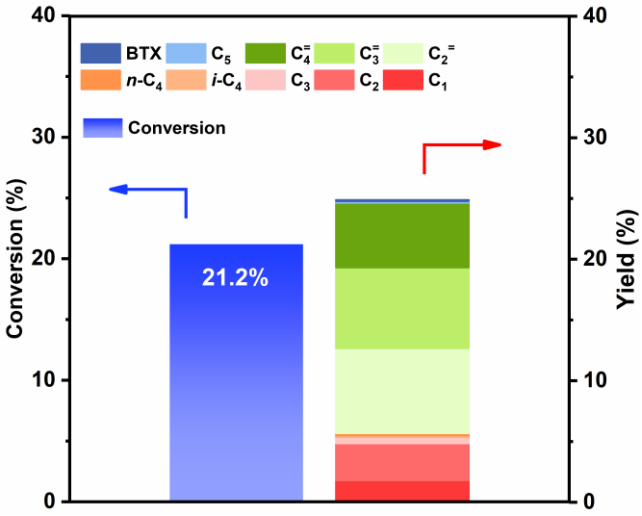

Fig. S39 Conversion and product distributions for thermal cracking, under blank test at 873 K in the absence of catalyst with 0.02 mL min^{-1} *n*-heptane volume flow rate.

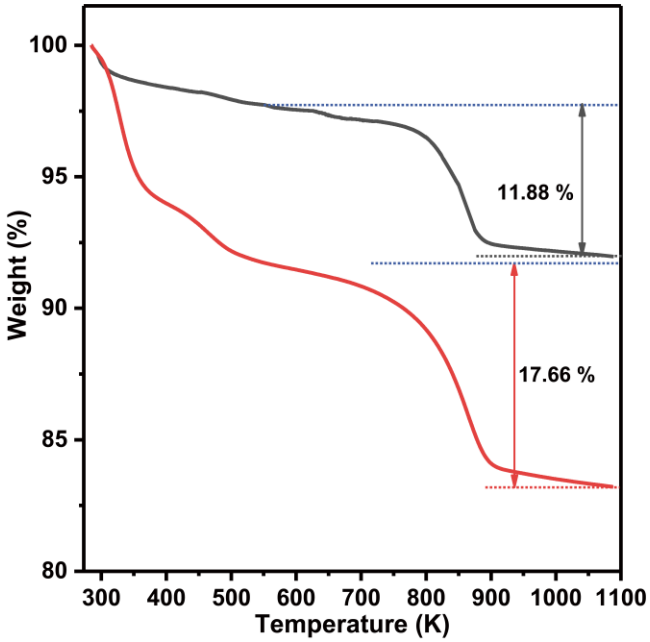

Fig. S40 TGA measurements of deposited coke over spent catalysts.

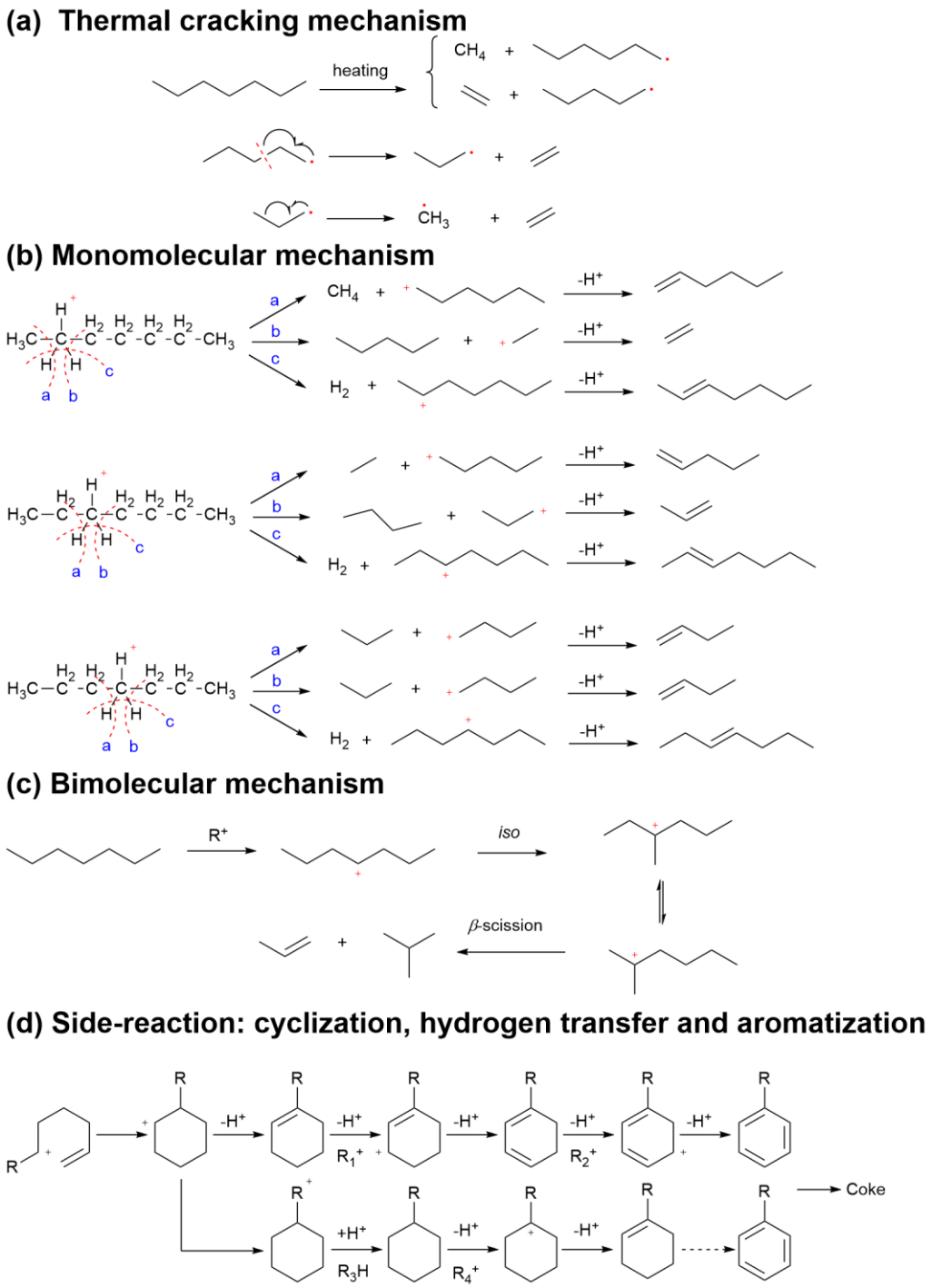

Scheme S1. The thermal cracking mechanism[5] (a) and catalytic cracking mechanism of *n*-heptane.[6-8] (b) monomolecular mechanism, (c) bimolecular mechanism, (d) side-reaction: cyclization, hydrogen transfer and aromatization.

4. Supplementary Video

Video S1. Sequence of x stacks from electron tomography of ZSM5-NPr_2-C_6-(50).

5. References

1. C. A. Emeis, *J. Catal.*, 1993, **141**, 347–354.
2. H. Ding, J. Ding, W. Liu, X. Zhao, Q. Chi, K. Zhu, X. Zhou and W. Yang, *CrystEngComm*, 2019, **21**, 577–582.
3. A. Hwang, D. Prieto-Centurion and A. Bhan, *J. Catal.*, 2016, **337**, 52–56.
4. S. Hovmöller, *Ultramicroscopy*, 1992, **41**, 121–135.
5. F. G. Helfferich, in *Comprehensive Chemical Kinetics*, ed. F. G. Helfferich, Elsevier, 2001, vol. 38, pp. 261–297.
6. R. Javaid, K. Urata, S. Furukawa and T. Komatsu, *Appl. Catal. A-Gen.*, 2015, **491**, 100–105.
7. A. Corma and A. V. Orchillés, *Microporous and Mesoporous Mater.*, 2000, **35-36**, 21–30.
8. V. Blay, B. Louis, R. Miravalles, T. Yokoi, K. A. Peccatiello, M. Clough and B. Yilmaz, *ACS Catal.*, 2017, **7**, 6542–6566.